Satellite observations of ozone in the upper mesosphere

A. K. Smith,[1] V. L. Harvey,[2] M. G. Mlynczak,[3] B. Funke,[4] M. García-Comas,[4] M. Hervig,[5] M. Kaufmann,[6] E. Kyrölä,[7] M. López-Puertas,[4] I. McDade,[8] C. E. Randall,[2,9] J. M. Russell III,[10] P. E. Sheese,[11] M. Shiotani,[12] W. R. Skinner,[13] M. Suzuki,[14] and K. A. Walker[11]

Received 18 November 2012; revised 22 April 2013; accepted 25 April 2013; published 10 June 2013.

[1] Ozone profiles in the upper mesosphere (70–100 km) retrieved from nine instruments are compared. Ozone from the Sounding of the Atmosphere using Broadband Emission Radiometry (SABER) instrument is used as the basis of comparison. Other measurements are from the Halogen Occultation Experiment, the High Resolution Doppler Imager, the Michelson Interferometer for Passive Atmospheric Sounding, the Global Ozone Monitoring by Occultation of Stars, the Atmospheric Chemistry Experiment—Fourier Transform Spectrometer, the Solar Occultation For Ice Experiment, the Optical Spectrograph and InfraRed Imaging System, and the Superconducting Submillimeter-Wave Limb-Emission Sounder. Comparisons of each data set with SABER using coincident profiles indicate agreement in the basic vertical profile of ozone but also some systematic differences in daytime ozone. Ozone from the SABER 9.6 μm channel is higher than the other measurements over the altitude range 60–80 km by 20–50%. Nighttime comparisons indicate better relative agreement (<10% difference). Taking all the data, not limited to coincidences, shows the global and seasonal distributions of ozone in the upper mesosphere from each instrument. The average maximum in ozone mixing ratio is around 90–92 km during daytime and 95 km at night. There is a maximum in ozone density at night (∼90 km) and during some hours of the day. The latitude structure of ozone has appreciable variations with season, particularly in the tropical upper mesosphere. The basic latitude-altitude structure of ozone depends on local time, even when the analysis is restricted to day-only observations.

Citation: Smith, A. K., et al. (2013), Satellite observations of ozone in the upper mesosphere, *J. Geophys. Res. Atmos.*, *118*, 5803–5821, doi:10.1002/jgrd.50445.

1. Introduction

[2] Ozone is a key observation from the Sounding of the Atmosphere using Broadband Emission Radiometry (SABER) instrument on the Thermosphere, Ionosphere, Mesosphere Energetics, and Dynamics (TIMED) satellite. Day and night observations of ozone are needed to address one of the central goals of the TIMED mission: to describe the energy balance of the mesosphere and lower thermosphere (MLT). Absorption of solar ultraviolet radiation by ozone is an important heating process there as elsewhere in the middle atmosphere. Ozone also participates in some of the exothermic reactions that convert the energy absorbed by O_2 and O_3 into heat.

[3] In this study, we use observations of ozone by SABER and eight other satellite instruments to assess the consistency of the distribution of global ozone among them. The focus is on the altitude region 70–100 km. Over periods of 2 months, the accumulated SABER observations cover all local times; most of the other available observations have a more limited local time range due either to limitations in

[1]Atmospheric Chemistry Division, National Center for Atmospheric Research, Boulder, Colorado, USA.
[2]Laboratory for Atmospheric and Space Physics, University of Colorado Boulder, Boulder, Colorado, USA.
[3]NASA Langley Research Center, Hampton, Virginia, USA.
[4]Instituto de Astrofisica de Andalucía, Granada, Spain.
[5]GATS, Inc., Driggs, Idaho, USA.
[6]Forschungszentrum Jülich, Jülich, Germany.
[7]Finnish Meteorological Institute, Helsinki, Finland.
[8]Department of Earth and Space Science and Engineering, York University, Toronto, Ontario, Canada.
[9]Also at Department of Atmospheric and Oceanic Sciences, University of Colorado Boulder, Boulder, Colorado, USA.
[10]Center for Atmospheric Sciences, Hampton University, Hampton, Virginia, USA.
[11]Department of Physics, University of Toronto, Toronto, Ontario, Canada.
[12]Research Institute for Sustainable Humanosphere, Kyoto University, Uji, Japan.
[13]Space Physics Research Laboratory, University of Michigan, Ann Arbor, Michigan, USA.
[14]Japan Aerospace Exploration Agency, Sagamihara, Japan.

Corresponding author: A. K. Smith, Atmospheric Chemistry Division, National Center for Atmospheric Research, PO Box 3000, Boulder, CO 80307, USA. (aksmith@ucar.edu)

2169-897X/13/10.1002/jgrd.50445

Table 1. Information for the Satellite Instruments Considered, in Order of Launch Date[a]

Instrument	Version	Years	Latitudes	Local Times at Eq	Day or Night	Resolution
HALOE	19	1991–2005	80°S–80°N		sunrise/sunset	2.3 km
HRDI	12	1994–2005	72°S–72°N	precessing	D	2.5 km
SABER 9.6 μm	1.07	2002–2012	83°S–83°N	precessing	D/N	2 km
SABER 1.27 μm	1.07	2002–2012	83°S–83°N	precessing	D	2 km
GOMOS	5	2002–2011	global	22–23h	N	3 km
MIPAS	V4O	2008–2009	global	10h, 22h	D/N	4–8 km
OSIRIS	1	2002–2011	82°S–82°N	6h, 18h	D	1.2–2.5 km
ACE-FTS	3.0	2004–2012	74°S–74°N		sunrise/sunset	3–4 km
SOFIE	1.2	2007–2012	65°S–85°S and N		sunrise/sunset	1.8 km
SMILES	2.4	2009–2010	65°S–65°N	precessing	D/N	3 km

[a]The approximate local time of the profiles at the equator is given for data from sun-synchronous satellites except for solar occultation measurements. The years correspond to data available for this study. Resolution refers to the vertical resolution in the mesosphere.

the measurement technique or to the orbit of the satellite. The approach is to compare SABER ozone using coincident profiles with each of the other instruments in turn. This will give us grounds for an assessment of the measurements. Then we will present the global structure and seasonal variations of ozone in the upper mesosphere as determined from each of the instruments that has volume mixing ratio (vmr) data.

[4] This is not a validation paper. Instead, the goal is to compare the picture of global mesospheric ozone from each of instruments and, as much as possible, explain the major differences. There are two categories of differences between the different measurements: those due to differences that would occur due to systematic and random differences in coincident retrieved profiles and those due to differences in the sampling by each instrument. The two major components of the sampling differences are the calendar years and the local times of the observations.

[5] The retrievals relate observed spectral information to vertical profiles of the density of ozone, normally represented in units of number of molecules per cubic centimeter. From a practical point of view of comparing profiles, using density is difficult because it changes by orders of magnitude with altitude. If the density of the background atmosphere is known, ozone density is readily converted to vmr. In the comparisons that follow, vmr comparisons are emphasized but density comparisons are also shown.

[6] We present comparisons of SABER ozone data from two independent retrievals using emissions at 9.6 μm and 1.27 μm with ozone from other data sets that extend into the upper mesosphere and have been operating during at least part of the time of the SABER mission. In order of launch date, these are

[7] 1. Halogen Occultation Experiment (HALOE) on the Upper Atmosphere Research Satellite (UARS);

[8] 2. High Resolution Doppler Imager (HRDI) on UARS;

[9] 3. Michelson Interferometer for Passive Atmospheric Sounding (MIPAS) on the Envisat satellite;

[10] 4. Global Ozone Monitoring by Occultation of Stars (GOMOS) on the Envisat satellite;

[11] 5. Optical Spectrograph and InfraRed Imaging System (OSIRIS) on the Odin satellite;

[12] 6. Atmospheric Chemistry Experiment - Fourier Transform Spectrometer (ACE-FTS) on SCISAT-1;

[13] 7. Solar Occultation for Ice Experiment (SOFIE) on the Aeronomy of Ice in the Mesosphere (AIM) satellite; and

[14] 8. Superconducting Submillimeter-Wave Limb-Emission Sounder (SMILES) on the International Space Station.

[15] Since the comparisons in this paper are focused on ozone above 70 km, observations that do not extend to this altitude are not used. Data from the Microwave Limb Sounder (MLS) on the Aura satellite are not included; *Froidevaux et al.* [2008] show that the precision of retrieved ozone profiles drops sharply above 0.1 hPa. We also omit observations from data sets that terminate before 2000 (for example, from the Solar Mesospheric Explorer and the Cryogenic Infrared Spectrometers and Telescopes for the Atmosphere) and observations from ground-based instruments [e.g., *Hartogh et al*., 2004; *Rogers et al*., 2012].

[16] Section 2 gives more information about each of the data sets. The observational techniques include infrared emissions by ozone (9.6 μm for SABER and MIPAS), submillimeter emissions by ozone (SMILES), near-infrared emissions by O_2 (SABER at 1.27 μm; HRDI and OSIRIS at 762 nm), absorption by ozone using solar occultation in the infrared (HALOE and ACE-FTS) and ultraviolet (SOFIE), and stellar occultation in the ultraviolet (GOMOS). The connection between the ozone density and the measured radiance varies for the different techniques. Solar and stellar occultation is a first order relation because the absorption is almost entirely due to ozone molecules in the ground state. Thermal emission measurements give a less direct link. The emissions provide a measure of the excited state populations of ozone; some relationship is needed to get back to the ozone ground state and the total ozone number density. When the emitting state is not in local thermodynamic equilibrium (LTE), the relation is through the vibrational temperature. And, finally, airglow emission measurements are still further removed from ozone concentrations because of the assumptions about chemical equilibrium as well as the additional parameters needed to derive the ozone including Einstein coefficients, collisional quenching rates, photolysis rates, collisional energy exchange probabilities, and so forth. For all of the measurements considered here, there is additional measurement uncertainty due to uncertainties in the calibration and bandpass of the instrument, dependence of the retrieval on interfering species, insufficient spectroscopic data, and inaccurate pointing knowledge, to mention some of the most important.

[17] Although there have been extensive validation activities for some of the ozone data sets included here, those

validation and intercomparison studies are mostly confined to the stratosphere and lower mesosphere [e.g., *Brühl et al*., 1996; *Dupuy et al*., 2009]. For comparisons of SABER 9.6 μm ozone below 70 km, see *Rong et al.* [2009].

2. Data

[18] Table 1 shows a list of instruments used in this study and the geographical coverage, years, local times of measurements, and vertical resolution. For direct comparisons, all of the profiles from each data set are interpolated to an altitude grid with spacing of 1 km. Descriptions of most of these instruments and the techniques for measuring ozone are given by *Cracknell and Varotsos* [2012].

2.1. SABER

[19] SABER began acquiring scientific data in January 2002 and is still operating with nearly 100% duty cycle. SABER ozone is independently retrieved from two separate channels measuring different radiances; one at 9.6 μm and the other at 1.27 μm. These will be referred to as 9.6 μm ozone and 1.27 μm ozone, respectively.

[20] This study uses data from the Level 2A files of Version 1.07. The profiles are used up to 105 km. The vertical resolution is about 2 km. The TIMED satellite precesses such that, over a 60–65 day yaw period, data are available at almost all local times (9.6 μm ozone) or all daytime hours (1.27 μm ozone). Day and night data are treated separately. The day/night flag in SABER has three settings: 0 for day, 1 for night, and 2 for partially illuminated. These settings are used to determine the category for each profile. The 1.27 μm ozone is available only for the day/night flag setting of 0. Some screening has been applied to the ozone values as described in section 2.1.3.

[21] Both ozone retrievals use the temperature and pressures derived from SABER observations; see *Remsberg et al.* [2008] for description and error analysis of SABER temperature. *Remsberg et al.* [2008] found that the SABER temperatures are in general too low by about 2 K in the middle mesosphere. The SABER temperature is also used in the conversion of units from ozone density to ozone vmr.

2.1.1. Retrieval of Ozone From the SABER 9.6 μm Emission Under Non-LTE Conditions

[22] SABER observes ozone emission in a bandpass from 1010 to 1150 cm^{-1} (9.9 to 8.7 μm). This interval was chosen to emphasize measurement of emission from the fundamental (001–000) band in the asymmetric stretch (ν_3) mode of ozone and to minimize emission from higher-lying hot bands. In the mesosphere and lower thermosphere, the entire ν_3 manifold departs from LTE. Analysis of ozone infrared emission measurements made by the Limb Infrared Monitor of the Stratosphere (LIMS) instrument [*Solomon et al.*, 1986] showed that the higher-lying ν_3 hot bands are chemically pumped. The significant uncertainty in the production and loss rates of these high-lying states may result in large uncertainty in the retrieved ozone concentration. LIMS and SABER are very similar instruments, and the experience from LIMS was essential in specifying a much narrower spectral bandpass for SABER.

[23] The retrieval of ozone requires a statistical equilibrium model of the vibrational states in the ground electronic state of the ozone molecule for the computation of vibrational temperatures of ozone. The vibrational temperatures are used in the computation of the radiance in the SABER spectral bandpass. The vibrational temperatures and the ozone abundances are updated iteratively in the retrieval process until convergence is achieved between measured and computed infrared radiances. An additional source of infrared radiance in the SABER bandpass is due to one of the two infrared laser bands of CO_2 [*Mlynczak and Drayson*, 1990a; *Edwards et al.*, 1996]. This emission is taken into account directly in the ozone retrieval using vibrational temperatures computed for CO_2 in the SABER temperature retrieval algorithm.

[24] The ozone vibrational temperature model is drawn from *Mlynczak and Drayson* [1990a, 1990b] and *Martin–Torres* [1999]. The SABER vibrational temperature model incorporates 133 vibrational states beginning at the $O_3(007)$ state 6850 cm^{-1} above ground and extends to the $O_3(000)$ ground state. These vibrational states comprise approximately 80% of the energy in the bound ozone molecule. The SABER model includes spontaneous emission of radiation (over 340 transitions), chemical pumping, collisional excitation, and quenching with N_2, O_2, and O, and radiative excitation in the ν_3 fundamental band using the computationally efficient approach defined by *Mlynczak and Drayson* [1991]. The collisional quenching rates for N_2 and O_2 are described by *Martin-Torres* [1999] and developed from the work of *Menard-Bourcin et al.* [1991]. The quenching rate for atomic oxygen was taken from *West et al.* [1976]. Collisional excitation is computed from the collisional quenching rates through detailed balance. A zero-suprisal distribution is used to specify the quasi-nascent distribution of chemically pumped energy in the states from 6850 cm^{-1} down to approximately 4500 cm^{-1} above ground. The abundance of atomic oxygen is provided from SABER measurements day and night [*Mlynczak et al*., 2013].

2.1.2. Ozone From the SABER 1.27 μm Emission

[25] The method for retrieving ozone from the SABER 1.27 μm retrieval is described by *Mlynczak et al.* [2007]. It is similar to that used to retrieve ozone from the Solar Mesosphere Explorer, which was launched in 1981 [*Thomas et al.*, 1984]. Figure 1 shows a schematic diagram of the path of energy from the absorption of solar radiation by ozone or O_2 to the emission of a 1.27 μm photon. The retrieval process thus needs to account for all the losses of energy, including quenching and spontaneous emissions. The rates used in the SABER retrieval are given by *Mlynczak et al.* [2007].

[26] As pointed out by *Mlynczak et al.* [2007], the Einstein spontaneous emission coefficient for the $O_2(^1\Delta)\rightarrow O_2(^3\Sigma)$ transition is 2.23×10^{-4} s^{-1}, or a lifetime of about 75 min. This means that the retrieved ozone represents the ozone from a fairly long-time interval that can extend more than an hour into the past. *Zhu et al.* [2007] showed that this time lag can cause errors in the ozone during periods when the concentration is changing rapidly. The times of rapid change include the periods near sunrise and sunset and also situations when the vertical winds are large. The latter is the case, for example, in tropical regions when the diurnal tide amplitude is large. Using a model, *Zhu et al.* [2007] estimated the difference between the time-dependent ozone and the ozone that would be in steady state, and hence consistent with the assumptions used in the 1.27 μm retrieval. The differences

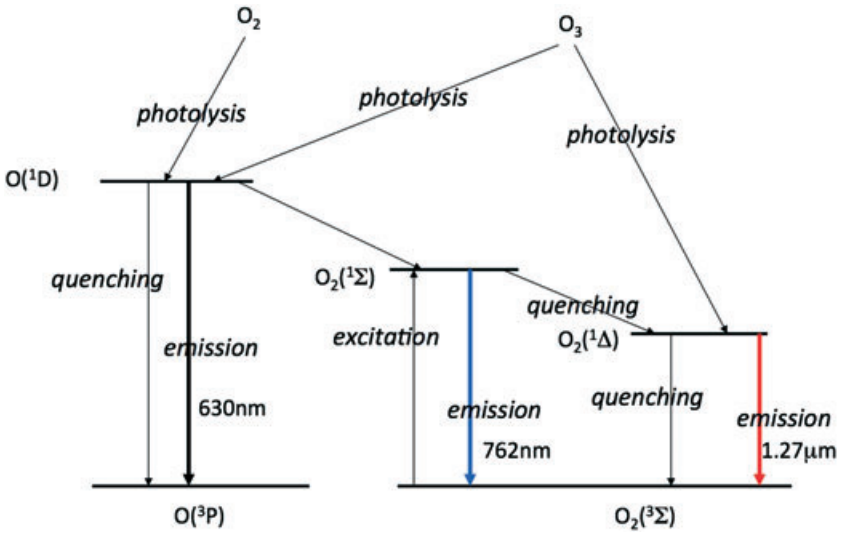

Figure 1. Schematic diagram of energy paths from the photolysis of O_2 or O_3 in the mesosphere. The red arrow indicates the 1.27 μm emission used to retrieve SABER daytime ozone. The blue arrow indicates the 762 nm emission used to determine daytime O_3 from HRDI and OSIRIS measurements. Adapted from *Mlynczak et al.* [1993].

vary strongly with local time and are largest after sunrise and before sunset. As a result, the ozone retrieved using the 1.27 μm emission could be overestimated by a factor of two in early morning and underestimated by a factor of two in evening.

[27] Comparisons (not shown) with other lower mesospheric ozone observations, including HALOE, ACE-FTS, and MLS Aura, indicate that the 1.27 μm ozone diverges from other observations below ∼60 km. This is outside the range investigated in the present study and so does not have an impact on the comparisons.

2.1.3. Screening of SABER Ozone Data

[28] *Smith et al.* [2008] showed in histogram form that the SABER v1.07 nighttime ozone can have outliers that appear to be unphysical. These rare outliers can occur when the interrelated ozone, atomic oxygen, and/or temperature retrievals do not converge due to corrupted radiance values or other data problems. Following the same approach, we determined the distribution of SABER ozone values for four different categories: 9.6 μm daytime ozone, 9.6 μm nighttime ozone, 1.27 μm daytime ozone (using only profiles with solar zenith angle (SZA) less than 75°), and 9.6 μm ozone under partially illuminated conditions (day/night flag=2).

[29] For each of the categories, the upper limit for screening is the value that separates the 0.1% highest values from the rest. The screening values are different at each altitude level but do not change with season or calendar year. Screening is applied separately at each altitude level so a profile may be partially screened. Application of a lower cutoff for vmr that were very low was also investigated but, in the upper mesosphere, the cutoff was indistinguishable from zero and so was not applied. The SABER retrievals do not allow negative vmr.

2.2. HALOE

[30] The HALOE, on the UARS satellite, provides solar occultation measurements of ozone and other molecules for the period 1991–2005. The instrument is described by *Russell et al.* [1993]. HALOE uses absorption of radiation at 10.04 μm for determining ozone. *Brühl et al.* [1996] show comparisons for the validation of the ozone measurements up to 0.01 hPa, about 80 km, from an earlier version. *Randall et al.* [2003] give a brief update for version 19, which is used in this study. HALOE ozone measurements have been extensively used for investigating the stratosphere [e.g., *Grooß et al*., 1999; *Remsberg*, 2009].

[31] The HALOE ozone profiles extend to 85–90 km with a vertical resolution of ∼2.3 km. For HALOE, as for other solar occultation instruments, sunrise and sunset profiles can have systematic differences and are considered separately.

2.3. HRDI

[32] The HRDI, on the UARS satellite, was designed to measure winds in the middle atmosphere. *Marsh et al.* [2002] describe the retrieval of daytime ozone from emissions by $O_2(^1\Sigma)$. Since UARS precesses in local time, HRDI provides one of the few global measurements of mesospheric ozone that spans many hours of local time.

[33] The HRDI ozone retrieval uses an emission at 0.76 μm; see the transition from $O_2(^1\Sigma)$ to the ground state, $O_2(^3\Sigma)$, on Figure 1. HRDI ozone is available from 62.5 to 97.5 km altitude with a vertical resolution of about 2.5 km. The current release is version 12. HRDI was operational from 1991 to 2005; ozone data span the period 1994–2005. For direct coincidence comparisons, we use the ozone observations for the period of overlap with SABER: 2002–2005. For presentation of the ozone climatology implied by the HRDI ozone measurements, we use the entire data record 1994–2005.

[34] Upper Atmosphere Research satellite suffered a loss of high quality attitude knowledge after the star trackers failed in mid-2000. After that time, information in the data was used to recover useful attitude knowledge, with some loss of accuracy but with satisfactory results. The procedure was to use the altitudes of the emission layers detected

by HRDI. The original attitude knowledge of UARS was 0.01°, which corresponds to an altitude uncertainty of about 0.5 km. The layer height of the emission layers is generally known to 1–1.5 km, giving an attitude knowledge of 0.02°–0.03°. This is still significantly smaller than the vertical field of view, 0.1° (5 km); so, although the altitude knowledge accuracy is somewhat reduced, the impact should be small. Also note that the overlap of HRDI with SABER occurred during the late stages of the UARS mission (after more than 10 years in orbit); as time went on, spacecraft power constraints increasingly reduced HRDI's duty cycle.

2.4. GOMOS

[35] *Bertaux et al.* [2010] give an overview of the GOMOS instrument, operation, data products, and scientific results. The basic measurement is stellar occultation. The technique for determining ozone profiles from GOMOS observations is described by *Kyrölä et al*. [2006, 2010a] and *Sofieva et al.* [2010]. *Kyrölä et al.* [2010b] show the temporal variation of ozone observed by GOMOS. *Tamminen et al.* [2010] give an analysis of errors in the retrieved products, including ozone.

[36] The GOMOS observations began in August 2002 and continued until April 2012. In February 2005, a technical problem led to a shut down for several months; data collection then resumed but with fewer profiles per day. A pointing problem that developed in 2009 further reduced the number of profiles available. We use the Level 2 data from version 5. GOMOS ozone profiles cover all latitudes and seasons; the local time of the measurements is around 22–23 h at low latitudes and has an extended range in high latitudes. The profiles extend up to 100 km and have a vertical resolution in the mesosphere of 3 km.

[37] Vertical profiles of temperature and local density in the MLT that are given in the GOMOS files are based on the empirical Mass Spectrometer Incoherent Scatter model. Because of the highly variable nature of the MLT region, these climatological values are not used in the present study. For coincident profiles, we use SABER background density for converting GOMOS ozone density to vmr.

[38] The ozone retrieval can vary depending on the star that is being observed and the geometry of the occultation measurement. *European Space Agency* [2007] recommends to screen profiles based on the star effective temperature, the star visual magnitude, the occultation obliquity, and the illumination condition. For accurate determination of mesospheric ozone, the star effective temperature is very important; the recommendation is to eliminate data from all stars with temperature less than 6000 K. However, *Kyrölä et al.* [2006] eliminated profiles from stars that have both a temperature of less than 7000 K and a magnitude greater than 1.9 (i.e., stars that are both cool and have low magnitude). In the screening applied here, we adapt both of these criteria and also screen out profiles with an occultation obliquity greater than 10°. Following *Kyrölä et al.* [2006], we discard daytime data and data near the dawn/dusk terminator by applying a minimum SZA cutoff of 108° to avoid possible problems with scattered light. Even with these screening limits, some extreme outliers remained. The outliers were removed following the same process as used for SABER (removing the highest 0.1%).

2.5. MIPAS

[39] The MIPAS provides measurements of the 9.6 μm emission for the retrieval of ozone. MIPAS also measures temperature simultaneously. Most of the MIPAS measurements were taken in the so-called nominal observation mode, ranging from about 6 to 70 km. In this paper, however, we use MIPAS measurements taken in the middle atmosphere mode (20–100 km) which have been used less frequently. Thus, during the first phase, September 2002–March 2004, characterized by the use of full spectral resolution (FR) (0.035 cm^{-1}), only a few orbits of measurements were taken. In the second MIPAS phase (starting in January 2005), characterized by the use of optimized spectral resolution (OR) (0.0625 cm^{-1}), these measurements were taken 30–40 days each year (distributed along all seasons) until the middle of 2007, and more frequently (average cadence of 2 out of 10 days) since late 2007 until 6 April 2012. Here, we use the MIPAS middle atmosphere ozone profiles version V4O_502, which are currently processed only for 2008 and 2009. The data were retrieved using the IMK/IAA processor developed at Institut für Meteorologie und Klimaforschung in Karlsruhe and the Instituto de Astrofisica de Andalucía in Granada [*von Clarmann et al*., 2003].

[40] *García-Comas et al.* [2012] give an evaluation of the MIPAS V4O_501 temperature retrievals, including comparisons with SABER and ACE-FTS, through the depth of the middle atmosphere. The MIPAS ozone retrieval and data validation from the FR measurements are described by *Gil-López et al.* [2005]; *Verronen et al.* [2005] show comparisons of MIPAS and GOMOS ozone in the MLT from 1 day each in 2002 and 2003. Version V4O_502 used here is based on OR spectra with different vertical sampling, resulting in slightly different precision and vertical resolution than those described in the works above. This version also uses an updated non-LTE O_3 model as described in *Funke et al.* [2012], including the improvements found in the study of MIPAS O_3 non-LTE spectra performed by *Kaufmann et al.* [2006]. As mentioned in section 2.1.1, atomic oxygen plays an important role in the vibrational excitation of O_3. Above 95 km, atomic oxygen is taken from the NRLMSIS-00 model [*Picone et al.*, 2002]. Below that altitude, atomic oxygen is assumed to be in photochemical equilibrium with ozone, and it is updated consistently within each retrieval iteration by means of a photochemical model based on the JPL 2007 recommendations [*Sander et al*., 2006] and atomic hydrogen concentrations from the NRLMSIS-00 model. Photolysis rates for O_2 and O_3 are calculated with the Tropospheric Ultraviolet and Visible (TUV) Radiation Model v4.3 [*Madronich and Flocke*, 1998] for the actual atmospheric condition.

[41] The MIPAS O_3 version V4O_502 has a vertical resolution (full width at half maximum of averaging kernel rows) of about 4 km below 75 km for both daytime and nighttime. Above this altitude, it is slightly coarser with values of 4–6 km at nighttime and 6–8 km at daytime. The precision (noise error) is smaller than 10% below 70 km, and 10–20% above 70 km, except for daytime where it reaches values of about 30% above 90 km. Screening rejects profiles with averaging kernel diagonals less than 0.03. In the analysis presented in this paper, profiles with SZA<85° are treated as daytime and those with SZA>95° as nighttime.

2.6. OSIRIS

[42] *Llewellyn et al.* [2004] describe the OSIRIS instrument and *Sheese* [2009] describes the retrieval of daytime mesospheric ozone from OSIRIS observations. The technique for determining ozone is similar to that used for HRDI, although the OSIRIS retrieval also includes the generation of $O_2(^1\Sigma)$ by the two-step Barth mechanism [*McDade et al.*, 1986]. Another difference is that the OSIRIS retrieval uses radiances integrated over the entire band whereas HRDI resolves individual rotational lines. The OSIRIS retrieval uses the Newtonian iteration optimal estimation technique of *Rodgers* [2008]. OSIRIS ozone is available only as density. Without simultaneous knowledge of the background atmospheric density in the mesosphere, there is no information to convert from ozone density to vmr. Odin is in a sun-synchronous orbit and the local time of the measurements is near the terminator. The daytime measurements used for ozone retrieval are only available in the summer hemisphere. The vertical resolution of the retrieved profiles is between 1.2 and 2.5 km.

[43] *Sheese* [2009] gives coincident comparisons of retrieved OSIRIS ozone density with SABER 9.6 μm and 1.27 μm observations for nine profiles distributed over a range of latitudes, local times, and years. The profiles generally agreed to within the combined uncertainties of the retrievals. In this study, we screen by omitting data with a low response of < 0.75. The response at each altitude is the sum of the rows of the averaging kernel matrix, as defined by *Rodgers* [2008], and is an indicator of the relative contributions of the measurements and the *a priori* data to a retrieved profile. Response values near zero indicate all *a priori*; values near one indicate that the *a priori* is not significant in the retrieval.

[44] In the present comparisons, we use all available OSIRIS-SABER coincidences for the period 2002–2011. The OSIRIS viewing schedule for the mesosphere has evolved during the mission. In early years, mesospheric measurements were made about 1 out of 10 days [*Murtagh et al*., 2002] but more recently this has changed to near-daily. Retrieved ozone profiles are currently available from July 2002 to February 2011.

2.7. ACE-FTS

[45] The Fourier Transform Spectrometer on the Atmospheric Chemistry Experiment has been making ozone observations since February 2004 [*Bernath et al*., 2005]. ACE-FTS solar occultation data are used to retrieve profiles of ozone and other molecules, along with temperature and pressure [*Boone et al.*, 2005]. Ozone profiles use radiance in the range 985–1128 cm^{-1} plus that at 922 cm^{-1}. *Dupuy et al.* [2009] present extensive comparisons of ACE-FTS ozone with other observations in the stratosphere and lower mesosphere. They found excellent agreement with other data. In this study, we use ACE-FTS version 3.0 for the period January 2004 through March 2012. ACE-FTS ozone profiles have a vertical resolution of 3–4 km and extend from ∼10 to ∼95 km.

2.8. SOFIE

[46] *Gordley et al.* [2009] and *Russell et al.* [2009] give introductions to the SOFIE instrument on AIM. Retrievals use solar occultation measurements to obtain sunrise and sunset profiles of temperature, pressure, ozone, and other trace gases. The AIM satellite has the specific task of measuring polar mesospheric clouds, which occur in high latitudes during summer. Because of the need to detect changes in cloud altitude, the instrument has high vertical resolution (1.8 km). The geographical sampling, which has been optimized for observing the atmosphere when these clouds are present, has a limited latitude range of approximately 65°–82° in both hemispheres. SOFIE retrieves ozone from measurements at 0.292 μm. Profiles have a lower limit of about 55 km due to saturation of the 0.292 μm band.

[47] SOFIE acquires ozone measurements during all seasons. Satellite occultation sunset (local sunrise) measurements are made in the Southern Hemisphere at ∼23 h local time and satellite occultation sunrise (local sunset) measurements in the Northern Hemisphere at ∼1 h local time.

2.9. SMILES

[48] The SMILES operated for 6 months, from 12 October 2009 to 21 April 2010. *Kikuchi et al.* [2010] give an overview of the mission and present some early results. *Imai et al.* [2013] present comparisons of SMILES ozone version 2.1 below 80 km with other measurements, including SABER 9.6 μm, ACE-FTS, and MIPAS.

[49] The latest version of SMILES (version 2.4) is used here. In this version, there is a new ozone retrieval that provides values to higher levels in the mesosphere. The nominal latitude coverage is from ∼36°S to ∼65°N; there are also a few observations between 65° and 36°S. The vertical resolution in the mesosphere is about 3 km. Profiles are available up to ∼98 km. The temperature and pressure profiles that are needed to convert the data from density to vmr are taken from Goddard Earth Observing System Model, Version 5 (GEOS-5) assimilation data. The assimilation includes temperature from the Aura Microwave Limb Sounder (MLS). Above the level of GEOS-5, the MLS temperatures are used.

[50] Retrieved ozone profiles are available from two different channels of SMILES, the A and B bands. *Imai et al.* [2013] show that the differences between these ozone products are within 3% over the altitude range 20–67 km. In this study, the data from the two bands are combined. SMILES data with a negative precision flag are omitted. Profiles with SZA<85° are treated as daytime and those with SZA>95° as nighttime.

3. Comparisons of Mesospheric Ozone Using Coincident Profiles

[51] Coincidence profiles are determined for SABER and each of the other instruments. Coincidences for each pair of instruments have a different distribution of calendar days, local times, and latitudes, depending on various factors.

[52] The times of the available profiles vary between measurements. Some data sets have a limited range in local time. There are two reasons for this. (1) Satellites in a sun-synchronous orbit will pass a particular latitude at two local times per day, on the ascending and descending segments of the orbits; these local times vary with latitude but remain nearly constant over the course of the mission. Due to different viewing directions, instruments on the same satellite can have different mea-

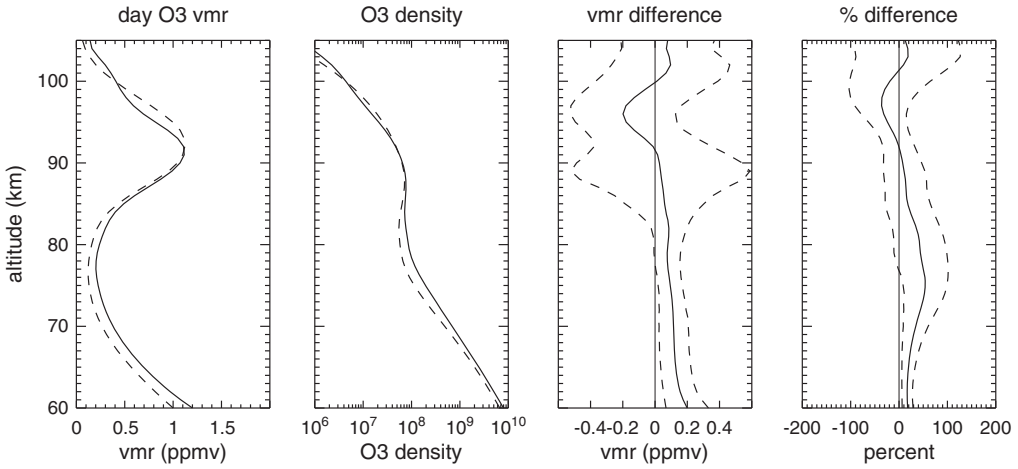

Figure 2. Profiles of ozone vmr (first panel; units ppmv) and ozone density (second panel; units cm^{-3}) from SABER 9.6 μm (solid) and 1.27 μm (dashed) retrievals averaged over all seasons and latitudes for January 2002–July 2012. The difference profiles show absolute difference (third panel; ppmv) and relative difference (fourth panel; %) for the 9.6 μm ozone minus the 1.27 μm ozone. The dashed lines give ± the de-biased standard deviation.

surement local times. (2) Some measurement techniques are possible only for a limited range of solar time. In particular, the measurement techniques used for SABER 1.27 μm emission, HRDI and OSIRIS work only during daylight; the measurements by GOMOS are used only for night conditions; and the solar occultation measurements of HALOE, ACE, and SOFIE are possible only during satellite sunrise and sunset.

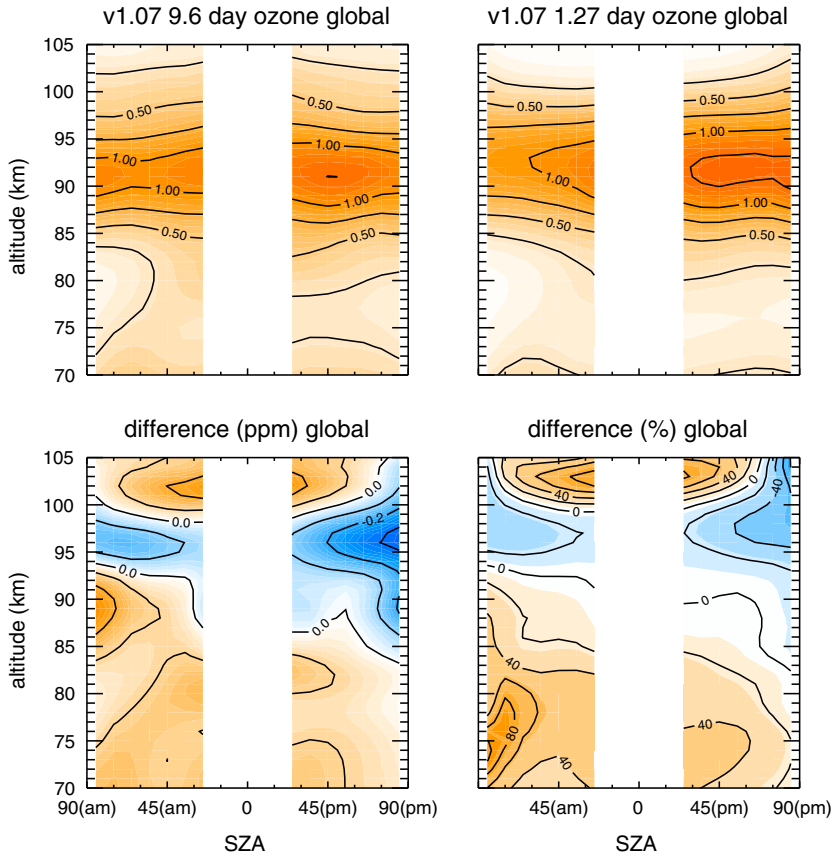

Figure 3. SABER daytime ozone as a function of solar zenith angle and altitude. In each panel, morning is on the left and afternoon on the right. Top left is 9.6 μm ozone; top right is 1.27 μm ozone; bottom left is absolute difference (9.6 μm ozone minus 1.27 μm ozone) and bottom right is percent difference.

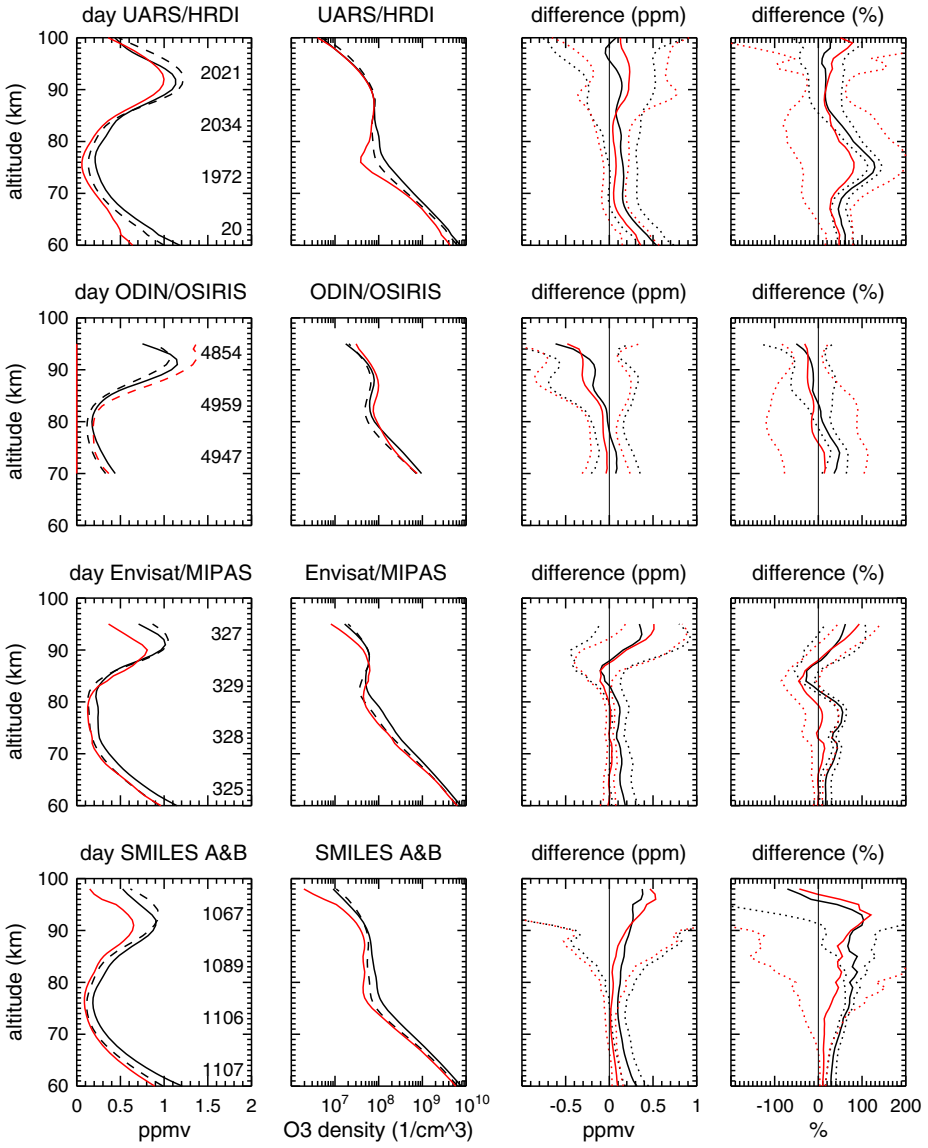

Figure 4. Profiles of ozone vmr (first column; units ppmv) and density (second column; units cm^{-3}) from coincident daytime measurements. Black is SABER (solid for the 9.6 μm retrieval and dashed for the 1.27 μm retrieval). Red is from HRDI (first row); OSIRIS (second row), MIPAS (third row), and SMILES (fourth row). OSIRIS vmr is shown as a dashed red line to indicate that SABER background density is used to calculate the vmr. The numbers along the right side of the vmr plots give the number of coincidences. The third and fourth columns give the absolute (units ppmv) and relative (%) differences (SABER 9.6 μm minus other instruments are black and SABER 1.27 μm minus other instruments are red). The dotted lines give ± the de-biased standard deviations.

[53] Table 1 gives the local times of measurements for all the data sets used in the comparisons. SABER 9.6 μm ozone and SMILES are the only data sets that cover the full local time range over a broad range of latitudes.

[54] In the upper mesosphere, the concentration of ozone is normally much higher during night than during day. In the coincidence comparisons that follow, we first separate the data into daytime and nighttime measurements. If both measurements are available for the pair of instruments being compared (only true for SABER 9.6 μm, MIPAS, and SMILES), then separate day and night comparisons are shown. For comparisons with the three solar occultation measurements, we use all SABER profiles that satisfy the coincidence criteria and are either in daylight (day/night flag = 0) or partially illuminated (day/night flag = 2). The coincident criteria are 200 km in horizontal distance and 1 h in universal time. For data sets that include negative ozone values (HRDI, GOMOS, ACE-FTS, and SMILES), these are included in the analyses.

[55] The comparisons are all given in vmr using the reported values, if available. In all cases, the measured radiance is more closely related to the ozone density than to the vmr. To perform the conversion, the profile of background total atmospheric density is also needed. ACE, HALOE, SOFIE, MIPAS, SABER, and HRDI each use background total density derived from simultaneous observations from

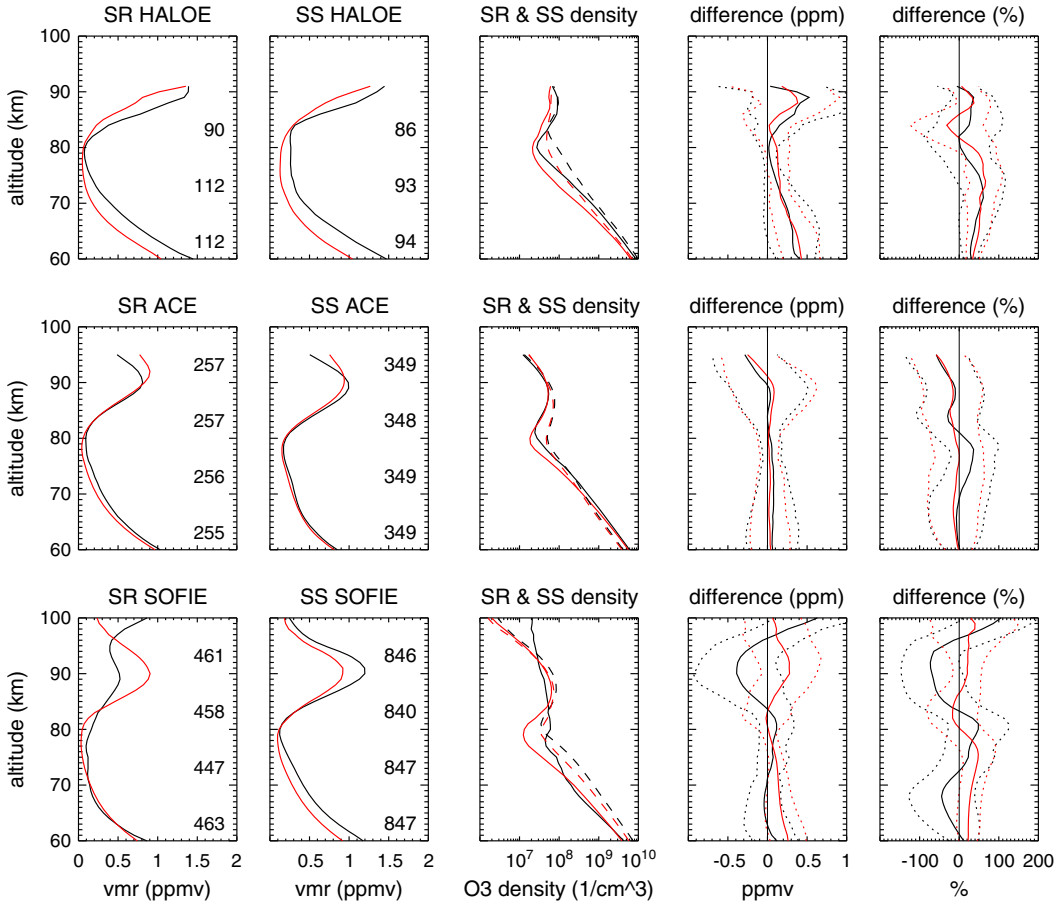

Figure 5. Profiles of ozone sunrise vmr (first column, ppmv), sunset vmr (second column, ppmv), and density (third column, cm^{-3}) from coincident measurements. Black is for SABER 9.6 μm. Red is for HALOE (top row); ACE-FTS (center row), and SOFIE (bottom row). SABER profiles have day/night flag=2 (partially illuminated). In the density plot, solid lines are for sunrise and dashed lines for sunset. The numbers along the right side of the vmr plots give the number of coincidences. The fourth and fifth columns give the absolute (units ppmv) and relative (%) differences (SABER 9.6 μm minus other instrument); black is for sunrise and red for sunset. The dotted lines give ± the de-biased standard deviations.

the same instrument. SMILES uses temperature derived or assimilated from a different satellite instrument (the Aura Microwave Limb Sounder) that operated at the same time. Since the data processing for each instrument was done separately, the background total densities used are not necessarily in agreement. Differences in background total densities can contribute to or offset differences in the profile comparisons. For this reason, we also compare the ozone densities directly.

[56] For GOMOS and OSIRIS, the background density is not available and therefore the vmr is not available. Instead, we convert ozone density to vmr using SABER background density from the coincident profile. The background number density n is determined from the pressure p and temperature T using the ideal gas law, $n = p/kT$, where k is Boltzmann's constant.

[57] For pairs of profiles that satisfy the coincidence criteria, the absolute differences at each level are calculated by [*Dupuy et al.*, 2009]

$$\delta_{abs} = X_{SABER} - X_{other} \quad (1)$$

and the relative differences by

$$\delta_{rel} = \frac{X_{SABER} - X_{other}}{(X_{SABER} + X_{other})/2} \quad (2)$$

For a total of N points, the mean difference for either absolute or relative is then

$$\Delta = \frac{1}{N}\sum_i \delta_i \quad (3)$$

The coincidence comparisons presented here show the mean absolute and relative differences. If negative mixing ratios are present, the mean and relative differences as calculated here can have different signs. An estimate of their combined precision is the de-biased standard deviation, σ, [*von Clarmann*, 2006] given by

$$\sigma = \sqrt{\frac{1}{N-1}\sum_i (\delta_i - \Delta)^2} \quad (4)$$

[58] Another parameter of interest is the standard error of the mean [*von Clarmann*, 2006], given by $\sigma/\sqrt{N}$. The standard error of the mean was calculated but is not included

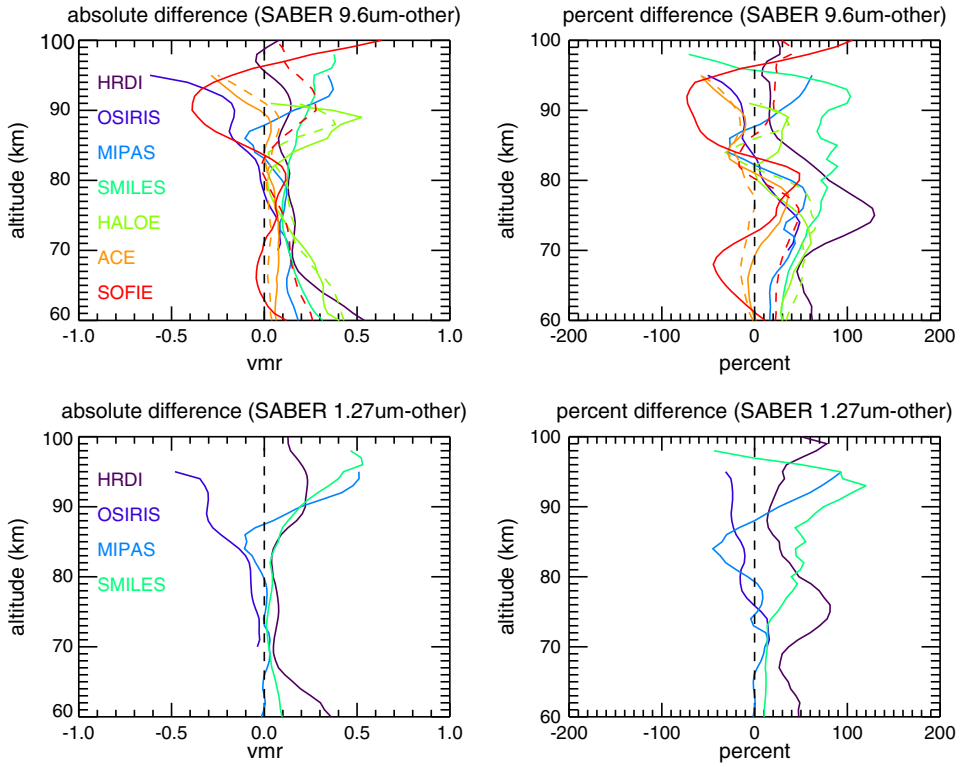

Figure 6. Top shows profiles of the absolute (left, units ppmv) and percentage (right) differences (SABER 9.6 μm ozone minus the other instrument) for SABER and seven other instruments from the coincident measurements shown in Figures 4 and 5. For the solar occultation cases (HALOE, ACE-FTS, and SOFIE), solid lines are for sunrise and dashed lines are for sunset. Bottom shows profiles of the absolute (left) and percentage (right) differences between SABER 1.27 μm ozone and four other instruments from the coincident measurements shown in Figure 4.

on the figures because its magnitude is smaller than the line width.

[59] An analysis technique frequently used in diagnosing instrumental differences by comparing pairs of profiles is to apply smoothing to the data with higher vertical resolution, such as convolving the profiles with the effective averaging kernels of the other. This minimizes the differences due to vertical resolution resulting from field of view, *a priori* information applied in the retrieval, scanning motion, or other factors. For example, *Verronen et al.* [2005] used this in comparing MIPAS and GOMOS mesospheric ozone. However, this technique is not used in the present study. Here, we want to keep the focus on what each instrument tells us about ozone in the upper mesosphere. Vertical resolution is one of many factors that affect the picture of ozone deduced from a particular measurement. The overall question is, even given all of the measurement differences, can we obtain a consistent result that allows for a consensus view of ozone in the upper mesosphere? In the discussion that follows, we will point out known differences, such as those in vertical resolution and in the local time of the observations, that have a predictable impact on the comparisons.

3.1. Comparisons of the Two SABER Daytime Ozone Retrievals

[60] For a comparison of the two SABER ozone retrievals, we take the profiles from the same scans, so the effective coincidence limits are zero. Both are screened as described in section 2.1.3. Figure 2 shows the profile comparisons and gives the standard deviations of the vmr. It is clear that there are systematic differences that exceed the standard deviations. In particular, the 9.6 μm ozone is higher than the 1.27 μm ozone between 60 and 85 km. The altitudes of the vmr peaks near 90–95 km are slightly offset; the 1.27 μm ozone peaks about 1–2 km higher.

[61] Figure 3 compares the two daytime SABER ozone retrievals as a function of SZA. The overall differences seen in Figure 2, particularly the difference below 85 km (where the 9.6 μm ozone is higher), are evident at all SZA. The magnitude of the percentage differences is larger in the morning hours at SZA>75°. As discussed in section 2.1.2, this is likely due to the long lifetime of $O_2(^1\Delta)$, which gives a systematic error to the retrieved 1.27 μm ozone during times of rapid change, such as near sunrise and sunset. For this reason, the 1.27 μm ozone for SZA>75° is not used in the remainder of the comparisons and analyses.

3.2. Daytime Coincidence Comparisons

[62] For the daytime comparisons, we differentiate between the solar occultation data, which are confined to sunrise and sunset, and the other observations. Figure 4 shows comparisons of SABER 1.27 and 9.6 μm daytime ozone with coincident profiles from HRDI, OSIRIS, MIPAS, and SMILES. The number of coincidences is indicated on

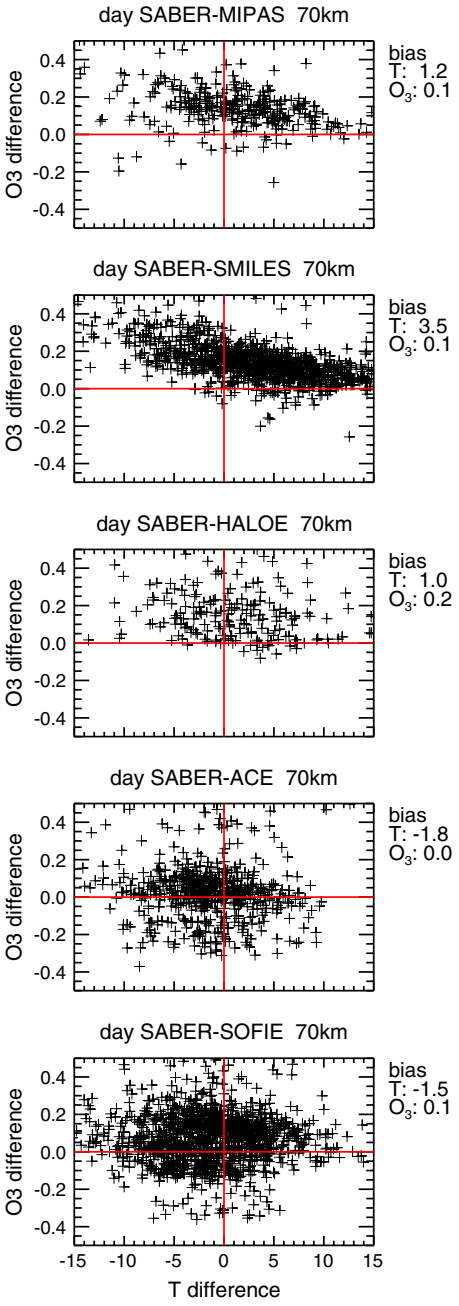

Figure 7. Scatter plot of the SABER minus other instrument temperature difference versus the ozone difference for each coincidence at 70 km. The panels are for SABER minus MIPAS, SABER minus SMILES, and so forth, using the SABER 9.6 μm ozone. The legend to the right gives the average temperature (K) and ozone (ppmv) differences for all daytime coincidences.

the figure; it varies greatly between the different pairs of instruments. HRDI, SMILES, and SABER are on precessing satellites, so the coincidences span a broad range of local times during daylight. MIPAS is on a sun synchronous satellite with daytime equatorial crossings at about 10 h local time. OSIRIS is also on a satellite with a sun synchronous orbit, but it is in approximately a dawn-dusk location. The times of the OSIRIS daytime profiles include local times during both morning and afternoon.

[63] The differences between the two SABER retrievals that were evident on Figure 2 are also apparent in the subset of profiles included here. The comparisons indicate that, below 80 km, the 1.27 μm ozone agrees better with all four of the other instruments.

[64] The slightly higher position of the ozone secondary maximum in the 1.27 μm retrieval that was apparent in Figure 2 is not as clear in the coincident profiles. Of the available daytime comparison data, HRDI, MIPAS, and SMILES extend high enough to resolve a well-defined maximum in the upper mesosphere. MIPAS puts the altitude of the daytime maximum at a lower altitude than either SABER profile, whereas the position of the maximum in HRDI and SMILES is consistent with both SABER profiles. Tests (not shown) indicate that the differences in vertical resolution between MIPAS and SABER (MIPAS has coarser resolution) affect the comparisons, particularly the altitude of the maximum. SABER profiles convolved with MIPAS averaging kernels have a lower position of the maximum than the fully resolved profiles; the position of the maximum in the convolved profiles is more consistent with that in the MIPAS profiles. Note that the retrievals from all of these instruments rely on non-LTE emissions and are therefore subject to errors from poorly known collisional parameters, radiative fluxes from below, or atmospheric conditions such as temperature and concentrations of other gases.

[65] We pay particular attention to the difference between SABER 9.6 μm daytime ozone and MIPAS ozone in the altitude range 60–82 km. The retrievals are based on the same emissions and, therefore, the contribution of retrieval parameters to the differences can be investigated. Such an investigation is currently underway. Preliminary tests indicate that SABER-MIPAS differences may be related to differences in parameters used for calculating the vibrational temperature.

[66] Ozone measured by solar occultation is often considered the standard because it is free from many assumptions that go into non-LTE retrievals. For these comparisons, we use SABER profiles with day/night flag=2 which means that the atmosphere is partially illuminated. With the fairly tight coincidence criteria used here (200 km and 1 h), there were few (HALOE) or no (ACE and SOFIE) coincidences with fully daylight profiles (SABER day/night flag=0). There are no available retrievals of the 1.27 μm ozone for day/night flag=2.

[67] Figure 5 compares coincidences with SABER 9.6 μm ozone profiles. Comparisons are segregated by local sunrise and sunset. Note that, for SOFIE, local sunrise corresponds to satellite occultation sunset and vice versa. The higher vmr of SABER 9.6 μm ozone below 80 km, noted with regard to comparison with other observations shown in Figure 4, is prominently seen in the sunrise and sunset HALOE comparisons and the sunset SOFIE comparisons; it is weakly evident in the ACE-FTS sunrise comparisons and absent in the sunset profiles of ACE-FTS and the sunrise profiles of SOFIE. From the density plots, it is evident that the ozone density from all three solar occultation instruments is substantially lower at sunrise than sunset over the altitude range 70–85 km. For both sunrise and sunset, the vmr associated with the minimum in the density profiles at 80 km are very

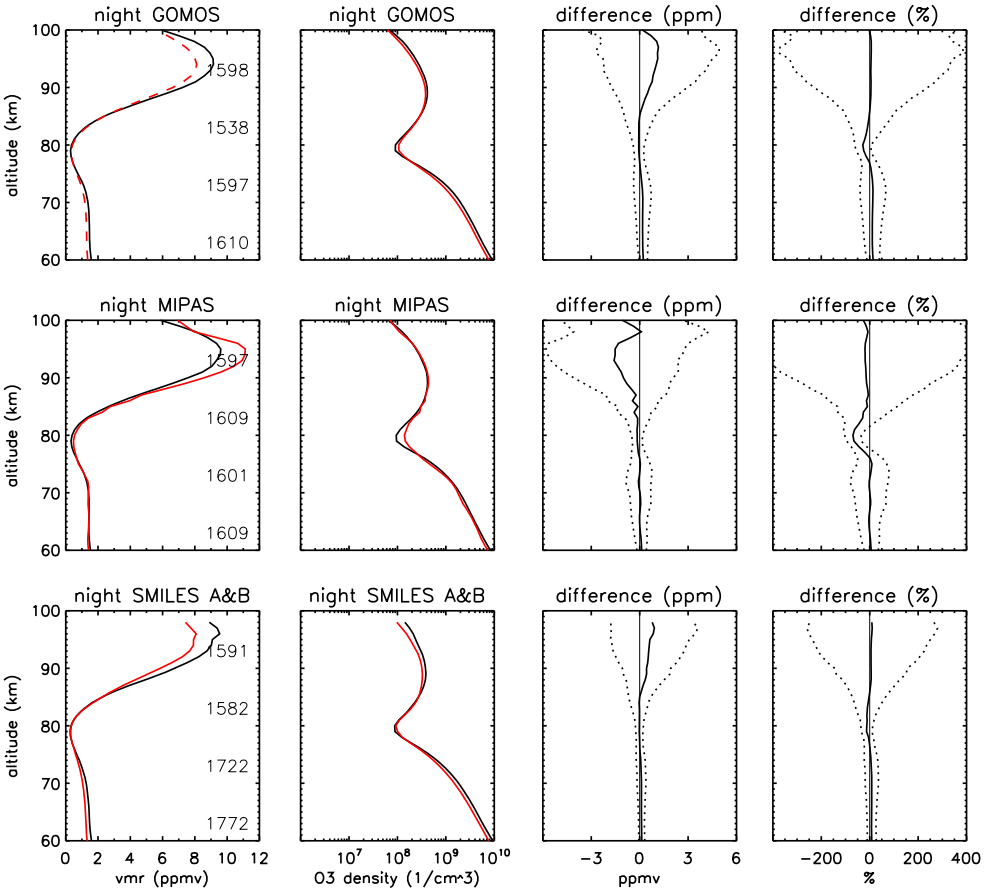

Figure 8. Profiles of ozone vmr (first column; units ppmv) and density (second column; units cm^{-3}) from coincident nighttime measurements. Black is for SABER 9.6 μm. Red is for GOMOS (top row), MIPAS (center row), or SMILES (bottom row). GOMOS vmr is given by a dashed line because SABER background density is used to calculate the approximate vmr. The numbers along the right side of the vmr plots give the number of coincidences. The third and fourth columns give the absolute (units ppmv) and relative (%) differences (SABER 9.6 μm minus other instrument). The dotted lines give ± the de-biased standard deviations.

low, less than 0.2 ppmv. The lifetime of odd oxygen is very short in this altitude range (see e.g., *Brasseur and Solomon* [2005]) so, at this local time, it is present mainly through transport from above or below.

[68] The SABER sunrise ozone profiles indicate a growth in the ozone vmr above about 97 km. Such an increase is not seen in other daytime profiles (c.f. Figure 4) and is not expected from considerations of photochemistry.

[69] Systematic differences are more easily viewed by overlaying the difference profiles (Figure 6). From the top panels, it is clear that the SABER 9.6 μm ozone over the altitude range 65–80 km is higher than that from all other instruments except SOFIE sunrise profiles. At higher altitudes, the scatter is larger and the number of instruments that have made observations is lower, so it is not so easy to identify systematic differences. Figure 6 also indicates

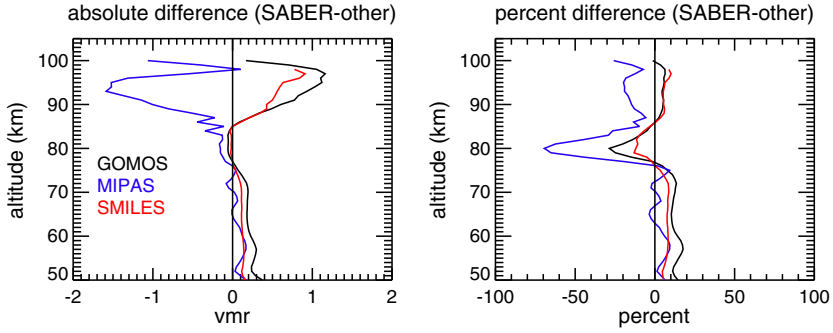

Figure 9. Profiles of the absolute (left, units ppmv) and percentage (right) differences (SABER ozone minus the other instrument) from the coincident measurements shown in Figure 8.

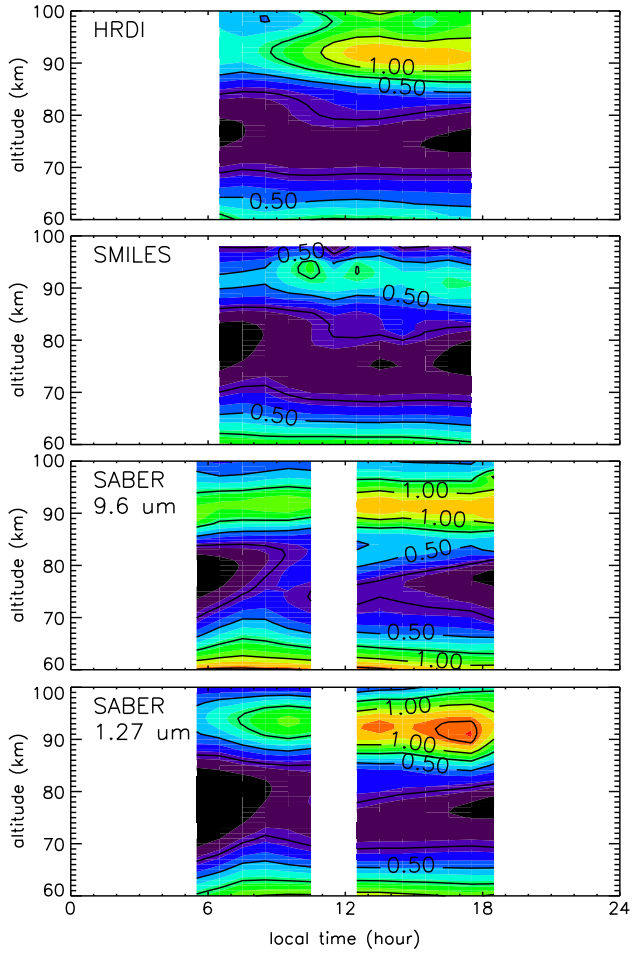

Figure 10. Local time × altitude cross sections of daytime ozone from HRDI, SMILES, and SABER averaged over the latitudes 15°S–15°N. Noon is at the center of the plot. Units are in ppmv. Contour interval is 0.25 ppmv.

that the difference between SABER ozone and that from other instruments at 60–85 km is somewhat reduced in the 1.27 μm ozone, as seen in Figure 4.

[70] *Rong et al.* [2009] showed positive differences between SABER daytime 9.6 μm ozone in the upper stratosphere and lower mesosphere and a number of other data sets. Their results are consistent with those presented here over the altitude range of overlap. *Rong et al.* [2009] note that the positive difference between SABER 9.6 μm ozone and other observations coincides in altitude with a negative temperature difference found by *Remsberg et al.* [2008]. To investigate this with the observations used in the present study, we show a scatter plot (Figure 7) of the temperature difference and ozone difference at 70 km for each coincident pair in the five cases for which we have daytime temperature and ozone data. For some of the pairs of coincidences, there is an apparent negative correlation. This likely results from the well-known negative correlation between ozone and temperature and reflects the fact that the coincident pairs are not viewing exactly the same atmospheric volumes. If the distribution of samples is randomly distributed, then the negative slope due to the chemically driven ozone-temperature correlation would persist, but there should be no net bias, and the sloped line would pass through the zero point. We focus on the net biases as a possible indicator of the reason for the ozone discrepancies shown in Figure 6. SABER 9.6 μm ozone is on average higher than MIPAS, SMILES, HALOE, and SOFIE ozone and has no average difference from ACE-FTS, consistent with the mean profiles in Figure 6. The mean ozone differences do not show a consistent relationship with the mean temperature differences, which can be positive (MIPAS, SMILES, and HALOE) or negative (ACE-FTS and SOFIE). Results at other altitudes are similar. This comparison does not point to kinetic temperature differences as being the leading cause of the systematic ozone differences.

3.3. Nighttime Coincidence Comparisons

[71] As indicated in Table 1, there are four nighttime data sets: SABER 9.6 μm, MIPAS, SMILES, and GOMOS. Figure 8 shows profile comparisons at the coincidences. Both the absolute and relative agreement of SABER 9.6 μm ozone with the other available observations is better during night than during day. This can also be seen in the difference plots (Figure 9).

[72] Discrepancies in the magnitude of the ozone maximum between SABER and MIPAS (Figure 8) are more evident in vmr than in density. Further investigation (not shown) indicates that about half of the difference (1 ppm at 92 km) is due to differences in the background density as determined from SABER and MIPAS temperature measurements. See *García-Comas et al.* [2012] for detailed comparisons of the SABER and MIPAS temperature differences.

4. Diurnal Variation of MLT Ozone From Observations

[73] To determine diurnal variation of global ozone, we use HRDI (daytime only) and SABER and SMILES (daytime and nighttime); these instruments are/were on precessing satellites. Because of the precession in local time, it takes about 35 days to accumulate full daytime coverage for HRDI; about 62 days for SABER; and about 30 days

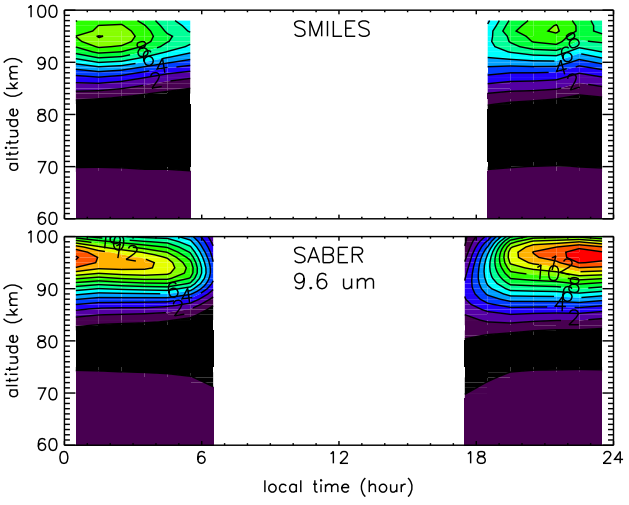

Figure 11. Local time × altitude cross sections of nighttime ozone from SMILES (top) and SABER (bottom) averaged over the latitudes 15°S–15°N. Units are in ppmv. Contour interval is 1 ppmv.

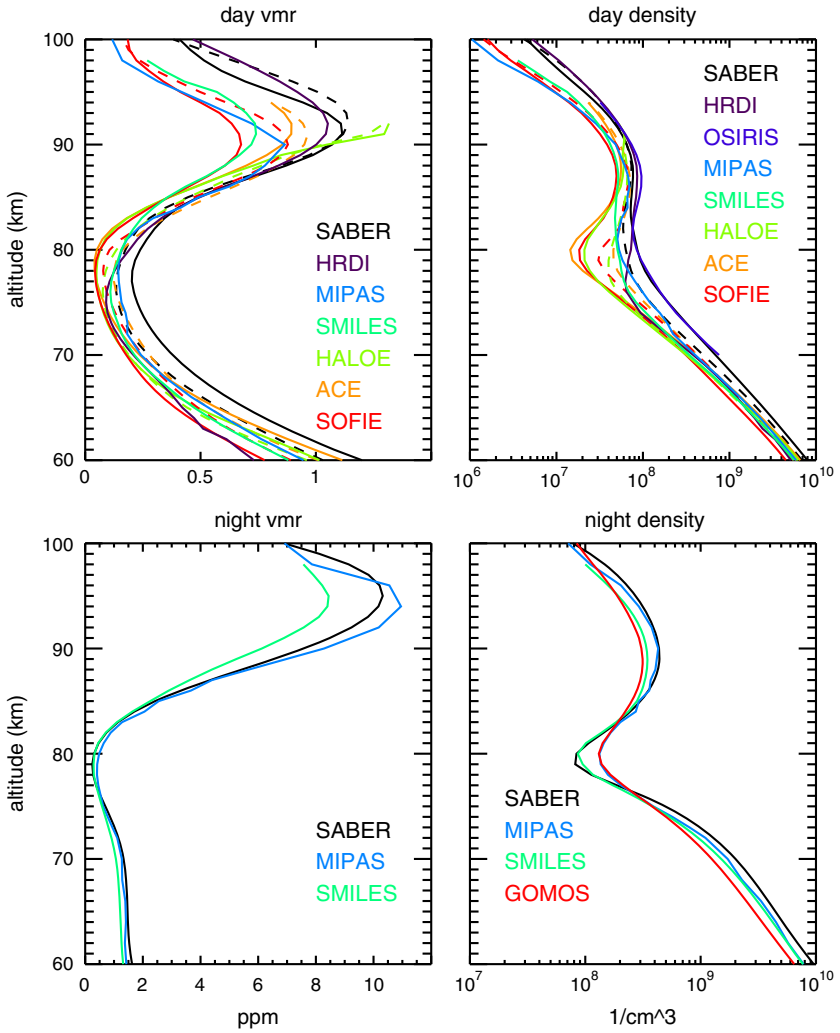

Figure 12. Left panels give the average of all ozone profiles for each of the instruments with vmr information. The right panels give the ozone density of all instruments used. For SABER, the solid lines are for 9.6 μm ozone and the dashed line is for 1.27 μm. For the solar occultation cases (HALOE, ACE-FTS, and SOFIE), solid lines are for sunrise and dashed lines are for sunset. Vmr units are in ppmv; density units are cm^{-3}.

for SMILES. SABER diurnal variations have also been presented by *Huang et al.* [2008], *Dikty et al.* [2010], and *Smith et al.* [2011]; HRDI diurnal variations have been presented by *Marsh et al.* [2002]. *Imai et al.* [2013] give comparisons of the diurnal cycles of ozone vmr as determined from SMILES and SABER.

[74] Figure 10 compares the daytime local time variation in low latitudes averaged over all seasons. All four panels indicate systematic local time variations in ozone during the daylight hours. *Marsh et al.* [2002] showed that the variations in the lower region (70–80 km) were due to photochemistry. Ozone concentration grows after sunrise due to increasing production, a side effect of O_2 photolysis. Later in the day, the destruction rate also increases due to catalytic cycles involving hydrogen and oxygen reactions. The timing of the maximum changes with local time is due to shifts in the photochemical processes. In the upper levels (above ~85 km), the daytime variation in ozone is tied to the migrating diurnal tide, particularly in low latitudes. The concentration of ozone is sensitive to temperature; the lowest concentration is simultaneous with the highest temperatures. Ozone variations are also affected by tidal transport of atomic oxygen but, at this altitude in the tropics, the temperature effect is dominant.

[75] SABER and SMILES are the only instruments capable of determining the local time variation during night. The SABER variation, shown in Figure 11, indicates a substantial local-time dependence in the upper mesosphere. This, like the local time variation at the same level during daylight, is associated with the migrating diurnal tide. Lowest temperatures and therefore highest ozone occur around midnight at this altitude [*Smith et al.*, 2008]. The magnitude of the nighttime variation measured by SMILES is smaller; in addition, it indicates a relative minimum in ozone near midnight. Further analysis (not shown) indicates that the differences in nighttime variation of the ozone maximum between SABER and SMILES are due in part to differences between the SABER measured temperature and the SMILES temperature taken from sun synchronous MLS measurements.

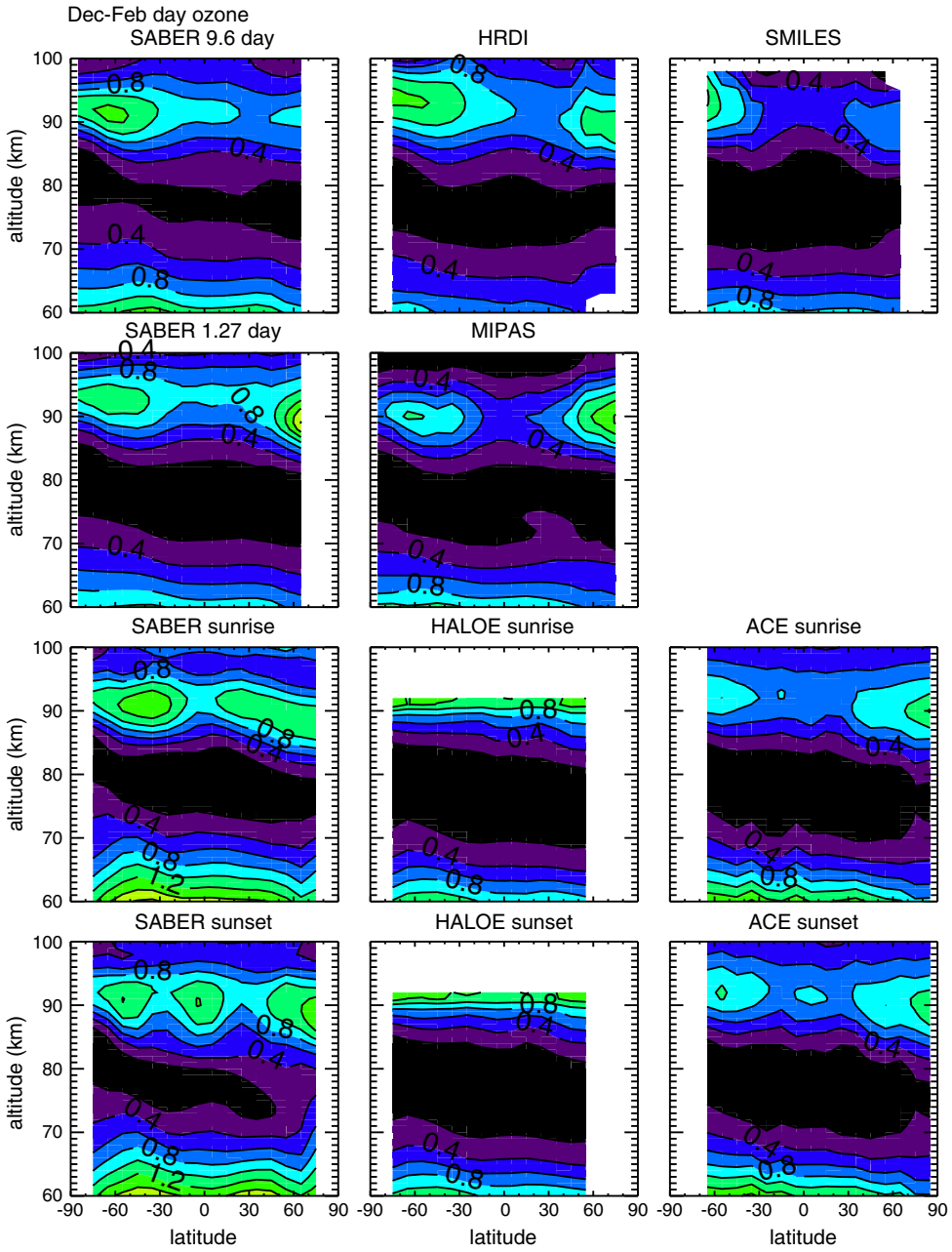

Figure 13. Average latitude × altitude distribution of daytime ozone vmr (ppmv) over all available years for the months December–February for each of the instruments with vmr information and sufficient latitude coverage. Four panels are given for SABER ozone: 9.6 μm for day, 1.27 μm for day, 9.6 μm for sunrise, 9.6 μm for sunset. For the solar occultation cases (HALOE and ACE-FTS), sunrise and sunset are plotted separately. Contour interval is 0.2 ppmv.

5. Global Distribution of MLT Ozone From Observations

[76] This section presents comparisons of the mean concentration and structure of ozone in the MLT determined from observations from each individual instrument. The goal is to assess how representative observations from a single instrument are and whether the overall picture of ozone from the different instruments is consistent. Ozone in the MLT region has not been well-constrained by observations up to now. Many differences between the observations have been noted in the previous sections. These include differences in the measurement techniques, instrumentation, retrieval methods, and vertical resolution. These differences account to a large extent for the differences when the coincidence criteria are narrow. There are also differences in the sampling that can lead to a different picture of the atmosphere even if the retrieved coincident profiles were to agree perfectly.

[77] For these comparisons, data are separated by day and night; solar occultation data are included in the daytime category. Differences due to sampling in local time are discussed. The entire available lifespan of each set of measurements is used; see Table 1 for the years included.

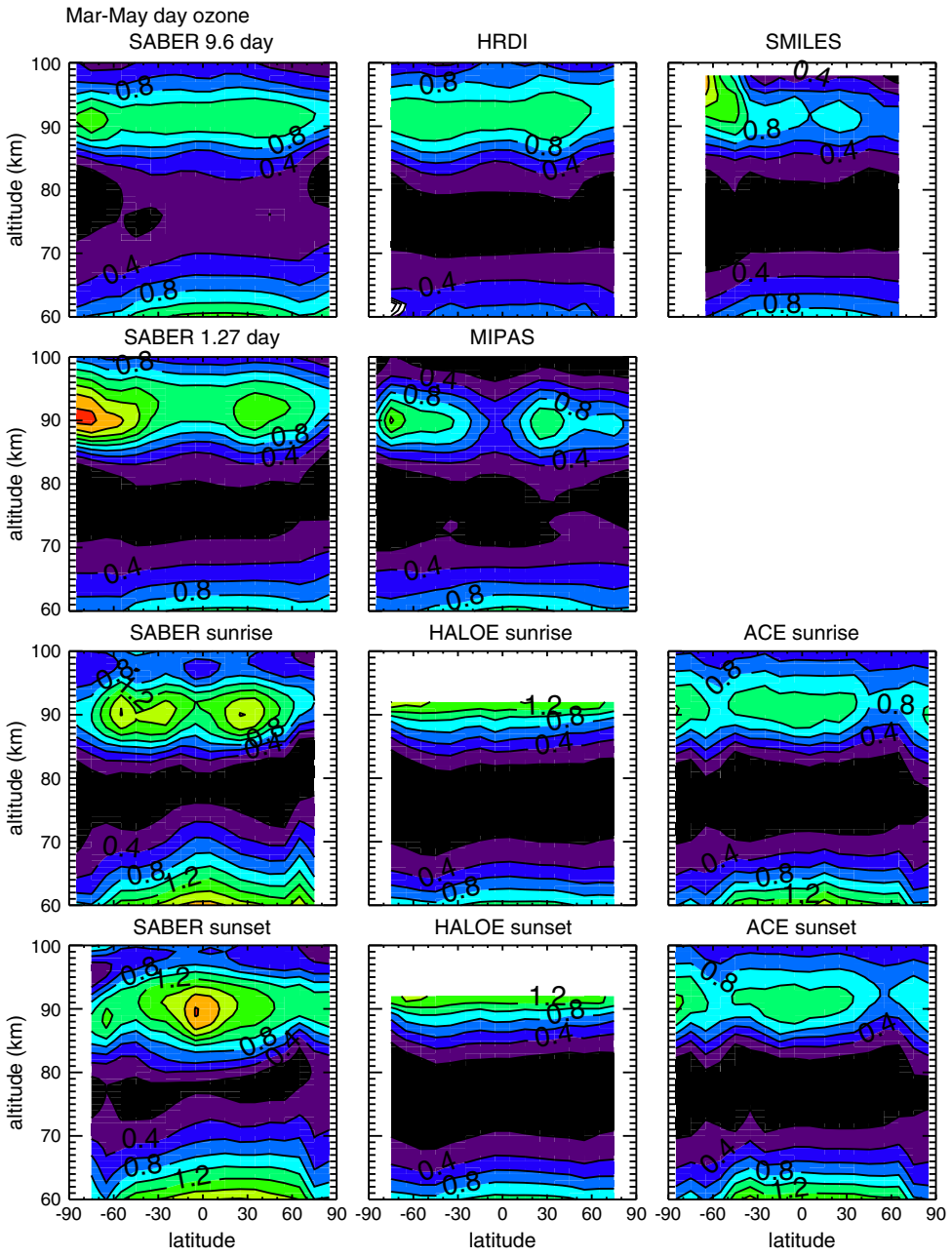

Figure 14. As in Figure 13 except the average over the months March–May. Contour interval is 0.2 ppmv.

5.1. Average Global Profiles

[78] Figure 12 shows the global annual mean daytime and nighttime ozone over the entire period available from each instrument. For this figure, there is no constraint to ensure that similar situations are being compared. In addition to measurement differences, factors that could contribute to ozone differences are local time, years, and latitudinal range of the measurements. Nevertheless, the comparisons reinforce some of the features seen in the coincidence comparisons (Figures 4–9). For example, the SABER 9.6 μm ozone is consistently higher than most of the other measurements. The ozone vmr decreases above about 90–92 km. However, there is a broad spread of the mean values and gradients.

[79] Some of the differences can be traced to sampling. All three solar occultation measurements indicate a pronounced minimum in ozone around 80 km, particularly at sunrise, that is not evident in other types of data. Referring back to the coincidence comparisons in section 3, we see that SABER 9.6 μm ozone has a similar deep minimum in vmr and density when coincident with the solar occultation data (Figure 5), but a much less pronounced minimum when coincident with midday (MIPAS) or precessing (HRDI and SMILES) ozone. This is an indication that the deep minimum is a feature of sunrise and sunset, not a characteristic of all daytime profiles.

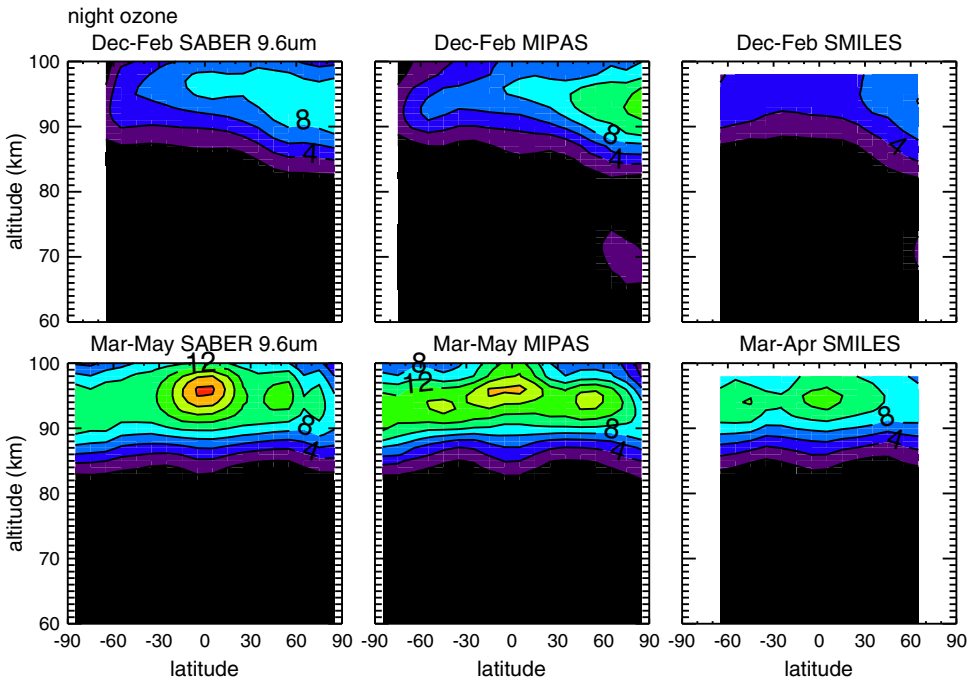

Figure 15. Average latitude × altitude distribution of nighttime ozone vmr (ppmv) over all available years for the months December–February (top) and March–May (bottom) for the instruments with vmr information. Contour interval is 2 ppmv.

[80] Comparison of the nighttime ozone distributions from SABER, MIPAS, and SMILES indicates very similar values and vertical gradients below 86 km.

5.2. Seasonal and Latitudinal Structure

[81] Figure 13 shows the latitude versus altitude cross section of daytime ozone vmr for the solstice period December–February, denoted DJF. The data have been sorted into 10° latitude bins and averaged over these months. SOFIE cross sections are omitted because the latitudinal coverage is not sufficient to generate a plot. OSIRIS ozone is omitted because there is no vmr data from this instrument.

[82] While the distributions are not identical, there are nevertheless some strong similarities among the 11 panels. The altitude of the deep minimum in ozone slopes downward from the summer hemisphere to the winter hemisphere. The high ozone at the secondary maximum (90 km) is not uniform with latitude but has a relative minimum in low latitudes and has relative maxima in middle or high latitudes of both hemispheres.

[83] There are also differences that confirm expectations for ozone. The local minimum at the equator around 90–95 km coincides with the altitude region where the phase of the diurnal tide in temperature has its maximum near midday. Note that the minimum is deeper for MIPAS (midday measurements) and SABER, HRDI, and SMILES daytime measurements (all daytime hours) than for the SABER sunrise/sunset and solar occultation data.

[84] Figure 14 shows the daytime latitude versus altitude structure for the equinox season March–May (MAM). During this period, differences between the ozone distributions from different instruments are much more evident. The ACE-FTS solar occultation measurements at sunrise/sunset indicate an ozone maximum in the low latitude upper mesosphere. SABER measurements at sunset also have an equatorial maximum, although sunrise measurements instead indicate a relative minimum at the equator. The latitude structure of measurements at other sunlit times (top two rows) also indicates a relative minimum at the equator. This is a local time rather than instrument effect, as seen by the different patterns in the SABER measurements at different local times.

[85] The difference between the latitude structure during DJF and MAM is consistent with the expected role of the migrating diurnal tide. The tidal amplitudes are much larger during equinox season, particularly around March–April, and have a dominant impact on the structure of ozone. Tidal temperature perturbations affect chemical reaction rates (lower T gives higher photochemical equilibrium O_3), and tides also transport atomic oxygen and hydrogen. These processes have canceling impacts so the sign and magnitude of the response of ozone to tides varies with altitude, latitude, and season.

[86] Figure 15 shows the nighttime ozone latitude versus altitude structure during DJF and MAM from SABER, MIPAS, and SMILES. The distributions determined from the three instruments are similar during both seasons, although the amount of ozone is lower in the SMILES observations. The weak ozone maximum in MIPAS vmr during DJF is the tertiary ozone maximum [*Marsh et al.*, 2001], which is not apparent in the SABER or SMILES observations. The ozone maximum at the equator during MAM is another indication of the response of ozone to the migrating diurnal tide.

6. Conclusions

[87] Measurements of ozone in the upper mesosphere over the past two decades from nine different instruments on seven satellites are now available. Comparisons of coincident profiles verify that many features of ozone agree among the different data sets. Features that agree are the following:

[88] 1. Ozone is much more abundant during night than during day;

[89] 2. The altitude of the secondary maximum in ozone mixing ratio is 90–92 km during day and 95 km at night. The altitude of the secondary maximum in density is 85–90 km during day and 90 km at night; and

[90] 3. Ozone is very low (<0.2 ppm) at about 80 km during both day and night. A minimum in ozone density occurs at sunrise at 80 km.

[91] There are also some discrepancies between different observations.

[92] 1. SABER 9.6 μm daytime ozone is higher than most other measurements over the altitude range 60–85 km.

[93] 2. There is a large range of values of daytime ozone above 90 km among all available measurements that may represent measurement uncertainties, systematic biases, retrieval differences, and differences in vertical resolution or may be a symptom of large geophysical variability.

[94] Recall that some of the mixing ratio differences may reflect differences in the background atmosphere used to determine mixing ratio from ozone density. The effect is not local because the background number density depends on pressure as well as temperature. As an estimation of the magnitude of this effect, considering only the local temperature (i.e., neglecting pressure differences), profiles with the same ozone density but different temperatures would have ozone mixing ratios that differ by the ratio of the temperatures.

[95] The second step in the comparisons is to determine what we can say about the global structure of MLT ozone, including its diurnal, latitudinal, and seasonal variations, from the available measurements. For this, we use the coincidence comparisons mentioned above and also look at all the observations from each instrument, without regard for coincidences between instruments. The analysis shows that the vertical structure and seasonal variations determined from different instruments can be substantially different even when coincident comparisons indicate good agreement. This is due to sampling differences. Here we have emphasized the sampling in local time as strongly affecting the implied global ozone, even when the data are restricted to day-only or night-only. Local time affects ozone through photochemical changes associated with the diurnal cycle in SZA, particularly below about 82 km, and through tidally induced changes in temperature and atomic oxygen, primarily above 85 km. Other differences that can contribute to differences in the overall ozone concentrations are different years of sampling, particularly different phases of the solar cycle, and different seasonal pattern of latitude coverage.

[96] The distribution of ozone determined from these measurements indicates seasonal and latitude variations in the magnitude and structure of ozone at the secondary maximum.

[97] 1. The latitudinal structure of daytime ozone varies with the time of day of the measurements.

[98] 2. At midday, ozone has a relative minimum at low latitudes and has maxima in middle or high latitudes of both hemispheres.

[99] 3. The ozone structure determined from sunrise measurements differs from that of sunset measurements.

[100] 4. Nighttime ozone has a maximum near the winter pole during solstice seasons and a maximum at the equator during equinox seasons.

[101] **Acknowledgments.** The National Center for Atmospheric Research is sponsored by the National Science Foundation. Support for this work was also provided by the NASA Heliospheric Guest Investigator Program. The IAA team was supported by the Spanish MCINN under grant AYA2011-23552 and EC FEDER funds. MGC is financially supported by the MINECO under its Ramon y Cajal subprogram. The Atmospheric Chemistry Experiment (ACE), also known as SCISAT, is a Canadian-led mission mainly supported by the Canadian Space Agency and the Natural Sciences and Engineering Research Council of Canada. JEM/SMILES mission is a joint project of Japan Aerospace Exploration Agency (JAXA) and National Institute of Information and Communications Technology (NICT).

References

Bernath, P. F., et al. (2005), Atmospheric chemistry experiment (ACE): Mission overview, *Geophys. Res. Lett.*, *32*, L15S01, doi:10.1029/2005GL022386.

Bertaux, J. L., et al. (2010), Global ozone monitoring by occultation of stars: An overview of GOMOS measurements on ENVISAT, *Atmos. Chem. Phys.*, *10*, 12,091–12,148, doi:10.5194/acp-10-12091-2010.

Boone, C. D., R. Nassar, K. A. Walker, Y. Rochon, S. D. McLeod, C. P. Rinsland, and P. F. Bernath (2005), Retrievals for the atmospheric chemistry experiment Fourier-transform spectrometer, *Appl. Opt.*, *44*, 7218–7218.

Brasseur, G., and S. Solomon (2005), *Aeronomy of the Middle Atmosphere: Chemistry and Physics of the Stratosphere and Mesosphere*, 3rd ed., 646 pp., Springer, Heidelberg, Germany.

Brühl, C., et al. (1996), Halogen occultation experiment ozone channel validation, *J. Geophys. Res.*, *101*(D6), 10,217–10,240.

Cracknell, A. P., and C. Varotsos (2012), *Remote Sensing and Atmospheric Ozone: Human Activities Versus Natural Variability*, Springer, Berlin.

Dikty, S., H. Schmidt, M. Weber, C. von Savigny, and M. G. Mlynczak (2010), Daytime ozone and temperature variations in the mesosphere: A comparison between SABER observations and HAMMONIA model, *Atmos. Chem. Phys.*, *10*, 8331–8339., doi:10.5194/acp-10-8331-2010.

Dupuy, E., et al. (2009), Validation of ozone measurements from the Atmospheric Chemistry Experiment (ACE), *Atmos. Chem. Phys.*, *9*, 287–343.

Edwards, D. P., J. B. Kumer, M. López-Puertas, M. G. Mlynczak, A. Gopalan, J. C. Gille, and A. Roche (1996), Non-local thermodynamic equilibrium limb radiance near 10 μm as measured by UARS CLAES, *J. Geophys. Res.*, *101*, 26,577–26,588, doi:10.1029/96JD02133.

European Space Agency (2007), GOMOS Product Handbook 3.0 Paris, [Available at http://envisat.esa.int/handbooks/gomos/CNTR.htm].

Froidevaux, L., et al. (2008), Validation of Aura Microwave Limb Sounder stratospheric ozone measurements, *J. Geophys. Res.*, *113*, D15S20, doi:10.1029//2007JD008771.

Funke, B., M. López-Puertas, M. García-Comas, M. Kaufmann, M. Höpfner, and G. Stiller (2012), GRANADA: A Generic RAdiative traNsfer AnD non-LTE population algorithm, *J. Quant. Spectrosc. Radiat. Transfer*, *113*, 1771–1817, http://dx.doi.org/10.1016/j.jqsrt.2012.05.001.

García-Comas, M., et al. (2012), On the quality of MIPAS kinetic temperature in the middle atmosphere, *Atmos. Chem. Phys.*, *12*, 6009–6039, doi:10.5194/acp-12-6009-2012.

Gil-López, S., et al. (2005), Retrieval of stratospheric and mesospheric O_3 from high resolution MIPAS spectra at 15 and 10 μm, *Adv. Space Res.*, *36*, 943–951, doi:10.1016/j.asr.2005.05.123.

Gordley, L. L., et al. (2009), The solar occultation for ice experiment, *J. Atmos. Sol. Terr. Phys.*, *71*, 300–315, doi:10.1016/j.jastp.2008.07.012.

Grooß, J.-U., R. Müller, G. Becker, D. S. McKenna, and P. J. Crutzen (1999), The upper stratospheric ozone budget: An update of calculations based on HALOE data, *J. Atmos. Chem.*, *34*, 171–183.

Hartogh, P., C. Jarchow, G. R. Sonnemann, and M. Grygalashvyly (2004), On the spatiotemporal behavior of ozone within the mesosphere/mesopause region during nearly polar night conditions, *J. Geophys. Res.*, *109*, D18303, doi:10.1029/2004JD004576.

Huang, F. T., H. G. Mayr, J. M. Russell, M. Mlynczak, and C. A. Reber (2008), Ozone diurnal variations and mean profiles in the mesosphere, lower thermosphere, and stratosphere, based on measure-

ments from SABER on TIMED, *J. Geophys. Res.*, *113*, A04307, doi:10.1029/2007JA012739.

Imai, K., et al. (2013), Validation of ozone data from the Superconducting Submillimeter-Wave Limb-Emission Sounder (SMILES), *J. Geophys. Res.*, doi:10.1002/jgrd.50434, in press.

Kaufmann, M., et al. (2006), Vibrationally excited ozone in the middle atmosphere, *J. Atmos. Sol. Terr. Phys.*, *68*, 202–212, doi:10.1016/j.jastp.2005.10.006.

Kikuchi, K., et al. (2010), Overview and early results of the Superconducting Submillimeter-Wave Limb-Emission Sounder (SMILES), *J. Geophys. Res.*, *115*, D23306, doi:10.1029/2010JD014379.

Kyrölä, E., et al. (2006), Nighttime ozone profiles in the stratosphere and mesosphere by the Global Ozone Monitoring by Occultation of Stars on Envisat, *J. Geophys. Res.*, *97*, D24306, doi:10.1029/2006JD007193.

Kyrölä, E., et al. (2010a), Retrieval of atmospheric parameters from GOMOS data, *Atmos. Chem. Phys.*, *10*, 11,881–11,849, doi:10.5194/acp-10-11881-2010.

Kyrölä, E., et al. (2010b), GOMOS O_3, NO_2, and NO_3 observations in 2002–2008, *Atmos. Chem. Phys.*, *10*, 7723–7738, doi:10.5194/acp-10-7723-2010.

Llewellyn, E. J., et al. (2004), The OSIRIS instrument on the Odin spacecraft, *Can. J. Phys.*, *82*, 411–422, doi:10.1139/P04-005.

Madronich, S., and S. Flocke (1998), The role of solar radiation in atmospheric chemistry, in *Handbook of Environmental Chemistry*, edited by P. Boule, pp. 1–26, Springer, Heidelberg.

Marsh, D., A. Smith, G. Brasseur, M. Kaufmann, and K. Grossmann (2001), The existence of a tertiary ozone maximum in the high-latitude middle mesosphere, *Geophys. Res. Lett.*, *28*(24), 4531–4534, doi:10.1029/2001GL013791.

Marsh, D. R., W. R. Skinner, A. R. Marshall, P. B. Hays, D. A. Ortland, and J.-H. Yee (2002), High resolution Doppler imager observations in the mesosphere and lower thermosphere, *J. Geophys. Res.*, *107*(D19), 4390, doi:10.1029/2001JD001505.

Martin-Torres, J. (1999), Emisiones infrarrojas del ozono en la atmosfera de la tierra, PhD thesis, Univ. de Granada, Granada, Spain.

McDade, I. C., D. P. Murtagh, R. G. H. Greer, P. H. G. Dickinson, G. Witt, J. Stegman, E. J. Llewellyn, L. Thomas, and D. B. Jenkins (1986), ETON 2: Quenching parameters for the proposed precursors of $O_2(b^1\Sigma_g^+)$and $O(^1S)$ in the terrestrial nightglow, *Planet. Space Sci.*, *34*, 789–800.

Menard-Bourcin, F., J. Menard, and L. Doyennette (1991), Vibrational relaxation of ozone in O_3-O_2 and O_3–N_2 gas mixtures from infrared double-resonance measurements, *J. Chem. Phys.*, *94*(94), 1875.

Mlynczak, M. G., and S. R. Drayson (1990a), Calculation of infrared limb emission by ozone in the terrestrial middle atmosphere. 2. Emission calculations, *J. Geophys. Res.*, *95*, 16,512–16,521.

Mlynczak, M. G., and S. R. Drayson (1990b), Calculation of infrared limb emission by ozone in the terrestrial middle atmosphere. 1. Source functions, *J. Geophys. Res.*, *95*, 16,497–16,511.

Mlynczak, M. G., and S. R. Drayson (1991), Rapid computation of the radiative absorption rate in the ν_3 mode of mesospheric and lower thermospheric ozone, *J. Quant. Spectrosc. Radiat. Transfer*, *46*, 463–471.

Mlynczak, M. G., S. Solomon, and D. S. Zaras (1993), An updated model for $O_2(a^1\Delta_g)$ concentrations in the mesosphere and lower thermosphere and implications for remote sensing of ozone at 1.27 μm, *J. Geophys. Res.*, *98*, 18,639–18,648.

Mlynczak, M. G., B. T. Marshall, F. J. Martin-Torres, J. M. Russell III, R. E. Thompson, E. E. Remsberg, and L. L. Gordley (2007), Sounding of the atmosphere using Broadband Emission Radiometry observations of daytime mesospheric $O_2(^1\Delta)$ 1.27 μm emission and derivation of ozone, atomic oxygen, and solar and chemical energy deposition rates, *J. Geophys. Res.*, *112*, D15306, doi:10.1029/2006JD008355.

Mlynczak, M. G., et al. (2013), Atomic oxygen in the mesosphere and lower thermosphere derived from SABER: Algorithm theoretical basis and measurement uncertainty, *J. Geophys. Res.*, doi:10.1029/2012JD018754, in press.

Murtagh, D., et al. (2002), An overview of the Odin atmospheric mission, *Can. J. Phys.*, *80*(4), 309–319, doi:10.1139/P01-157.

Picone, J. M., A. E. Hedin, D. P. Drob, and A. C. Aiken (2002), NRLMSISE-00 empirical model of the atmosphere: Statistical comparisons and scientific issues, *J. Geophys. Res.*, *107*(A12), 1468, doi:10.1029/2002JA009430.

Randall, C. E., et al. (2003), Validation of POAM III ozone: Comparisons with ozonesonde and satellite data, *J. Geophys. Res.*, *108*(D12), 4367, doi:10.1029/2002JD002944.

Remsberg, E. E. (2009), Trends and solar cycle effects in temperature versus altitude from the Halogen Occultation Experiment for the mesosphere and upper stratosphere, *J. Geophys. Res.*, *114*, D12303, doi:10.1029/2009JD011897.

Remsberg, E. E., et al. (2008), Assessment of the quality of the Version 1.07 temperature-versus-pressure profiles of the middle atmosphere from TIMED/SABER, *J. Geophys. Res.*, *113*, D17101, doi:10.1029/2008JD010013.

Rodgers, C. D. (2008), *Inverse Methods for Atmospheric Sounding*, World Sci., Singapore.

Rogers, A. E. E., et al. (2012), Repeatability of the seasonal variations of ozone near the mesopause from observations of the 11.072-GHz line, *J. Atmos. Oceanic Technol.*, *29*, 1492–1504, doi:10.1175/JTECH-D-11-00193.1.

Rong, P. P., J. M. Russell III, M. G. Mlynczak, E. E. Remsberg, B. T. Marshall, L. L. Gordley, and M. López-Puertas (2009), Validation of Thermosphere Ionosphere Mesosphere Energetics and Dynamics/Sounding of the Atmosphere using Broadband Emission Radiometry (TIMED/SABER) v1.07 ozone at 9.6 μm in altitude range 15–70 km, *J. Geophys. Res.*, *114*, D04306, doi:10.1029/2008JD010073.

Russell, J. M., L. L. Gordley, J. H. Park, S. R. Drayson, A. F. Tuck, J. E. Harries, R. J. Cicerone, P. J. Crutzen, and J. E. Frederick (1993), The Halogen Occultation Experiment, *J. Geophys. Res.*, *98*, 10,777–10,797.

Russell, J. M., et al. (2009), The Aeronomy of Ice in the Mesosphere (AIM) mission: Overview and early science results, *J. Atmos. Sol. Terr. Phys.*, *71*, 289–299, doi:10.1016/j.jastp.2008.08.011.

Sander, S. P., et al. (2006), Chemical kinetics and photochemical data for the use in atmospheric studies. Evaluation number 15, *JPL Publ., 06-2,* Jet Propul. Lab., Calif. Inst. of Technol., Pasadena.

Sheese, P. (2009), Mesospheric ozone densities retrieved from OSIRIS observations of the O_2 A-band dayglow, PhD thesis, York Univ., Toronto, Ont., Canada.

Smith, A. K., D. R. Marsh, J. M. Russell III, M. G. Mlynczak, F. J. Martin-Torres, and E. Kyrölä (2008), Satellite observations of high nighttime ozone at the equatorial mesopause, *J. Geophys. Res.*, *113*, D17312, doi:10.1029/2008JD010066.

Smith, A. K., D. R. Marsh, M. G. Mlynczak, J. M. Russell III, and J. C. Mast (2011), SABER observations of daytime atomic oxygen and ozone variability in the mesosphere, in *Aeronomy of the Earth's Atmosphere and Ionosphere, IAGA Special Sopron Book Ser.,* vol. 2, edited by M. Abdu, D. Pancheva, and A. Bhattacharyya, pp. 75–82, Springer, Dordrecht, Netherlands.

Sofieva, V. F., et al. (2010), Retrievals from GOMOS stellar occultation measurements using characterization of modeling errors, *Atmos. Meas. Tech.*, *3*, 1019–1027, doi:10.5194/amt-3-1019-2010.

Solomon, S., J. T. Kiehl, B. J. Kerridge, E. E. Remsberg, and J. M. Russell III (1986), Evidence for nonlocal thermodynamic equilibrium in the ν_3 mode of mesospheric ozone, *J. Geophys. Res.*, *91*, 9865–9876.

Tamminen, J., et al. (2010), GOMOS data characterisation and error estimation, *Atmos. Chem. Phys.*, *10*, 9505–9519, doi:10.5194/acp-10-9505-2010.

Thomas, R. J., C. A. Barth, D. W. Rusch, and R. W. Sanders (1984), Solar Mesosphere Explorer near-infrared spectrometer: Measurements of 1.27-μm radiances and the inference of mesospheric ozone, *J. Geophys. Res.*, *89*, 9569–9580.

Verronen, P. T., et al. (2005), A comparison of night-time GOMOS and MIPAS ozone profiles in the stratosphere and mesosphere, *Adv. Space Res.*, *36*, 958–966, doi:10.1016/j.asr.2005.04.073.

von Clarmann, T. (2006), Validation of remotely sensed profiles of atmospheric state variables: Strategies and terminology, *Atmos. Chem. Phys.*, *6*, 4311–4320.

von Clarmann, T., et al. (2003), Retrieval of temperature and tangent altitude pointing from limb emission spectra recorded from space by the Michelson Interferometer for Passive Atmospheric Sounding (MIPAS), *J. Geophys. Res.*, *108*(D23), 4736, doi:10.1029/2003JD003602.

West, G. A., R. E. Weston, and G. W. Flynn (1976), Deactivation of vibrationally excited ozone by $O(^3P)$ atoms, *Chem. Phys. Lett.*, *42*, 488–493.

Zhu, X., J.-H. Yee, and E. R. Talaat (2007), Effect of dynamical-photochemical coupling on oxygen airglow emission and implications for daytime ozone retrieved from 1.27 μm emission, *J. Geophys. Res.*, *112*, D20304, doi:10.1029/2007JD008447.